



In-event surrogate model training for regional transmission tower-line system dynamic responses prediction in realistic hurricane wind fields

Xiao Zhu^a, Ge Ou^a, Zhaoxia Pu^b, Xin Li^b and Jiayue Xue^c

^aDepartment of Civil & Coastal Engineering, Engineering School of Sustainable Infrastructure & Environment, University of Florida, Gainesville, Florida, USA; ^bDepartment of Atmospheric Sciences, University of Utah, Salt Lake City, Utah, USA; ^cDepartment of Civil and Environmental Engineering, University of Utah, Salt Lake City, Utah, USA

ABSTRACT

Surrogate models have shown improved accuracy in predicting infrastructure responses during dynamic loadings. However, training a surrogate model for complex loading inputs across the entire hazard region remains challenging. This study provides insight into the training of surrogate models to estimate the responses of transmission tower-line structures in a coupled high-dimensional and high-resolution wind field and presents innovative methods for addressing these challenges. Four data- and physics-based spatial-temporal decoupling sampling methods are employed and cross-compared to obtain the most representative in-event wind profiles for training the surrogate model. Long Short-Term Memory (LSTM) is utilised as the surrogate model framework to predict the dynamic responses of the structure during the 2017 Hurricane Harvey. The accuracy and robustness of two transmission tower-line structure configuration surrogate models are validated by comparing the predictions with finite element analyses by using randomly distributed temporal and geospatial wind profiles throughout the hurricane. Finally, a single LSTM surrogate model is developed, trained by applying the full reference wind speed range of Hurricane Harvey for the regional-scale structural performance evaluation of the transmission tower-line system. The results demonstrate that the proposed surrogate model training methodology is general and can be applied to regional-scale structural performance evaluations.

ARTICLE HISTORY

Received 31 May 2023 Revised 5 February 2024 Accepted 9 February 2024

KEYWORDS

Long short-term memory; machine learning; regional hazard simulation; surrogate modelling; transmission towers; wind engineering

1. Introduction

The integrity of power network supporting structures is crucial for ensuring the stable and sustainable delivery of power from power plants to customers. Among all supporting structures, transmission tower-line structures are particularly vulnerable due to their location in various terrains and exposure to wind hazards. As the transmission network is an interconnected network composed of geographically distributed physical transmission towers, assessing structural performance at a regional scale is crucial. To ensure an accurate evaluation of regional-scale structure performance, it is important to use an appropriate structural analysis tool, in addition to accounting for the complex wind loading. To evaluate the performance of the transmission tower-line system under wind loading, physical law-governed structural analysis tools, particularly Finite Element Models (FEM) are believed to yield reliable and accurate results. However, the computational burden of FEMs increases dramatically with the expansion in scale and integration stability requirement (Chopra, 2012). Consequently, structural surrogate models have been proposed and validated to alleviate the computational burden of utilising numerical modelling in complex and large-scale engineering systems (Kroetz, Tessari, & Beck, 2017).

Among the various surrogate model configurations, the long short-term memory (LSTM) surrogate model is notable for capturing the high nonlinearity properties of the physical model, thereby accurately predicting the response timehistory. Zhang et al. (2019) were the first to apply an LSTM surrogate model to predict the displacement time-history of a real-world building under seismic loading. Zhang, Liu, and Sun (2020) further introduced a physics-informed LSTM surrogate model, which improved prediction accuracy in a three-story moment frame model compared with their first LSTM model. Im, Lee, and Cho (2021) proposed a POD-LSTM surrogate model, which combined the LSTM with proper orthogonal decomposition (POD) to solve the computational limitations of large-scale elasto-plastic FE models. The results showed that the proposed POD-LSTM is efficient and accurate in predicting the structural plastic strain and von Mises stress. Torky and Ohno (2021) presented a hybrid convolutional-LSTMs (ConvLSTM) model used for multi-input multi-output models, highlighting the importance of applying a data filtering technique to the input data. Liao, Lin, Zhang, and Wu (2023) introduced an

attention-based LSTM surrogate model to predict the seismic response of a bridge in cases of having limited training data.

While significant attention has been paid to constructing surrogate models for predicting the dynamic response of infrastructural structures (B. Li, Chuang, & Spence Seymour, 2021; B. Li & Spence Seymour, 2022; Mangalathu, Heo, & Jeon, 2018; Byung Kwan Oh, Glisic, Kim, & Park, 2019; B. K. Oh, Glisic, Park, & Park, 2020; Shin, Scott, Stewart, & Jeon, 2020; Z. Y. Wang, Pedroni, Zentner, & Zio, 2018), very few studies have concentrated on developing surrogate models for transmission structures under wind loading. Zhang, Song, and Shafieezadeh (2022) proposed an adaptive multi-fidelity GP reliability method for performing transmission tower reliability analysis, where transmission tower pushover analysis, considering the uncertainties of structural and static wind loading, is implemented to obtain the response defined for the limit state function. Jeddi et al. (2022) employed a gradient boost classifiers active learning method to derive the fragility curves of transmission towers under various natural hazards. The wind loading, adhering to the minimum design loads and associated criteria for buildings and other structures as specified in 7-22 (2022), is applied in a quasi-static manner over a one-minute loading window.

Xue, Xiang, and Ou (2021) proposed a convolutional neural network (CNN) model to predict the displacement of a free standing transmission tower under wind loadings. Xue and Ou (2021) demonstrated that the long short-term memory (LSTM) surrogate model could predict the dynamic responses of highly nonlinear transmission tower-line systems. From the literature review, the wind loading parameters used for calculating wind loading are derived from ASCE 7-22 (2022), where the calculation of wind speed along height employs either a power- or logarithmic-law. However, Yet, Li, Zhi, and Hu (2010) analysed wind speed data recorded at a meteorological tower and observed that the surface roughness coefficient varies with height and the mean wind speed at the reference height. Snaiki and Wu (2018) discovered that using power- or logarithmic-law wind profiles underestimates the effects of wind loading on tall buildings. Under the standard ASCE 7-22 (2022) assumptions, the variance in wind profile height is solely related to ground roughness, and independent of wind speed.

For structural response analysis at a regional scale, it is essential to consider realistic wind profiles within a specific event. High-fidelity and high-resolution realistic hurricane wind field data are accessible from the numerical weather prediction (NWP) community database. For instance, the TIGGE archive, comprising forecast data from thirteen global NWP centres starting from 2006 (TIGGE); and the Weather Research and Forecasting (WRF) model, capable of producing simulations based on actual atmospheric conditions from observations and analyses (WRF). The NWP database provides high-resolution wind profiles considering land types, temperature. However, the data from these meteorological models, containing millions of wind profiles for a region, present complexities that the wind profile

calculation methods stipulated by ASCE 7-22 (2022) cannot adequately describe.

In this paper, it is hypothesized that, during the same event, the spatial and temporal wind loading characteristics and their impact on transmission towers can be understood by selecting a limited set of training samples, namely an inevent surrogate model. This study aims to bridge gaps in the literature review by investigating the development of an in-event surrogate model for the transmission tower-line system. The objective of this model is to accurately predict the nonlinear time history of spatial-temporal wind loading during an evolving hurricane. The surrogate model utilises training data selected from the event and is expected to predict the response at specific temporal and spatial points of interest. The input to the model is the dynamic wind loading of a transmission tower-line model with thousands of degrees of freedom. Owing to the complexity of spatial-temporal correlated wind loading inputs, the intrinsic turbulence wind stochasticity is decoupled from the explicit wind profile characteristics. Given the complex wind profiles in a specific event, it is crucial to adopt an appropriate sampling strategy so that the sampled wind profiles can reveal the complexities hidden within the wind profile parametric space.

The study evaluates the effectiveness of in-event surrogate training in representing turbulence stochasticity and profile variation. The accuracy of the trained surrogate models is assessed by comparing the predicted and target displacement time histories using the root-mean-squared error (RMSE), cross-correlation coefficient, and peak displacement. Moreover, the robustness of the surrogate models is validated by predicting the structural dynamic responses from unseen wind profiles at other timestamps and widely geospatially distributed wind profiles in the numerical weather prediction (NWP) hurricane model. Finally, the study develops a single LSTM model trained across the full range of the in-event reference wind speed of the wind profiles to perform a regional-scale transmission tower-line performance assessment. In summary, this paper aims to: (1) adopt and evaluate different sampling methods to reveal the complexities hidden within the wind profile parametric space; (2) comprehensively assess the accuracy and robustness of surrogate models trained by different sampling methods by evaluating two transmission towerline structure configurations; (3) explore the adaptivity of applying surrogate models for regional-scale transmission tower-line performance evaluation.

The rest of the paper is organised as follows: In Section 2, the challenges related to the evaluation of hurricane-impacted power infrastructure performance are comprehensively discussed, and a proposed solution is presented. Section 3 introduces the Long Short-Term Memory (LSTM) architecture and details the four training algorithms utilised for selecting representative wind profiles. In Section 4, an evaluation is conducted to assess the accuracy, robustness, and scalability of a two-tower one-span surrogate model. Section 5 focuses on assessing the adaptivity of the proposed surrogate model training when applied to a new transmission tower-line

configuration. Finally, Section 6 presents the findings and conclusions.

2. Regional hurricane impacted power infrastructure performance problem

During a hurricane event, wind loads can become so extreme that they exceed the structural design capacities of infrastructure, particularly transmission towers, resulting in physical damage. This damage can alter the topology of the power network, which in turn leads to power delivery interruptions, commonly referred to as power outages. To assess the extent of damage to the power infrastructure caused by a hurricane, a framework has been devised, as depicted in Figure 1. Employing the framework proposed in Figure 1 necessitates an assessment of the characteristics of the intricate wind loading in hurricanes and the structural analysis tools required for response assessment.

2.1. Wind loading characteristics at a regional scale

Owing to the extensive length of the transmission tower-line system, the wind loadings it experiences are complex, and high-dimensional dynamic time histories. These loadings are spatially and temporally correlated, indicating their dependence on spatial location. Each time history consists of mean and turbulent wind speed components. When the analysis expands to a regional scale, the loading range broadens significantly, with the most critical factor being the widely distributed wind profiles across the entire region. This section will discuss the characteristics of realistic wind loading distribution in a regional-scale problem.

The dynamic wind speed at any node for a structure at any location is modelled as:

$$V_{ij}(x_{ij}, y_{ij}, z_{ij}, t) = V_{z,ij}(x_{ij}, y_{ij}, z_{ij}) + v_{ij}(x_{ij}, y_{ij}, z_{ij}, t)$$
(1)

The dynamic wind loading on the transmission tower infrastructure can be calculated as:

$$F_{ii}(x_{ii}, y_{ii}, z_{ii}, t) = 0.5 \rho V_{ii}(x_{ii}, y_{ii}, z_{ii}, t)^2 C_f A_m$$
 (2)

where $V_{ij}(x_{ij}, y_{ij}, z_{ij}, t)$ is the dynamic wind speed time history at the j^{th} node of the i^{th} power infrastructure; (x_{ij}, y_{ij}, z_{ij}) indicates the geographical coordinate of the corresponding node; $V_{z,ij}$ is the mean wind component at that node controlled by the wind profile; v_{ij} is the turbulent wind component calculated from the wind power spectrum; ρ is the air density; C_f is the drag coefficient; and A_m is the structural projected area. From the equation, it is intuitive that the complex wind loading across the entire region, V_{ij} , can be decoupled into the mean wind speed component $V_{z,ij}$ and turbulence wind component v_{ij} . The following sections will explain their characteristics in the regional infrastructural response simulation.

2.1.1. Regional wind profile characteristics in weather Research and forecast model

In conventional wind engineering applications, the mean wind speed at a given geographical location (x, y) varies along the vertical elevation and follows either a power-law:

$$\frac{V_z(z)}{V_r} = \left(\frac{z}{z_r}\right)^{\alpha} \tag{3}$$

where V_z is the mean wind speed at height z; V_r is the wind speed at reference height; z_r is the reference height, which is 10 m in ASCE 7-22 (2022); and α is the surface roughness coefficient.

Or a logarithmic law:

$$V_z(z) = \frac{V_*}{\kappa} In\left(\frac{z - z_d}{z_0}\right) \tag{4}$$

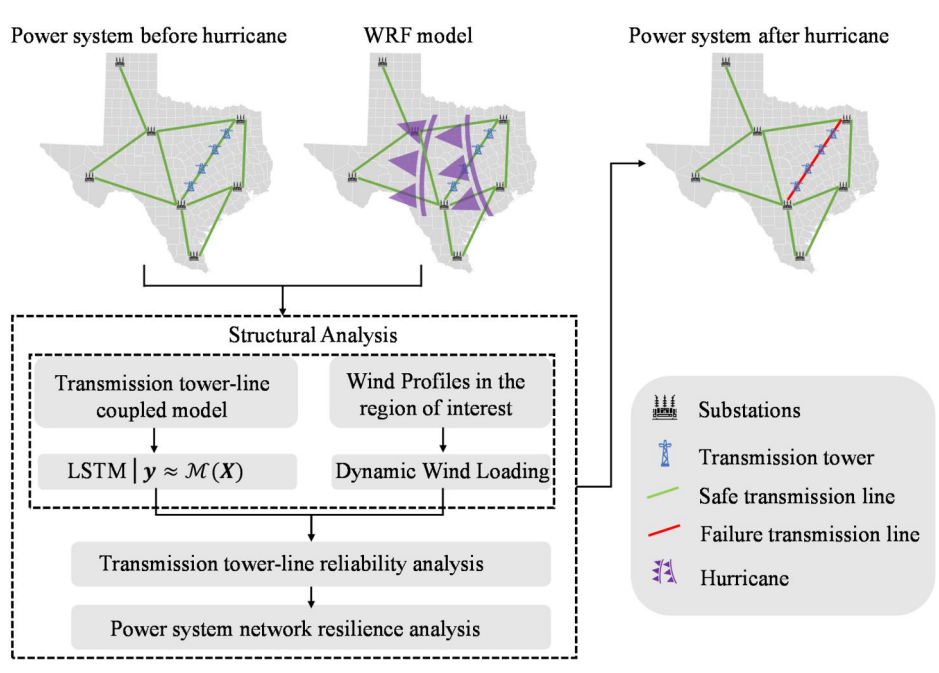


Figure 1. Schematic implementation of the proposed regional power system performance analysis framework during hurricane.

where V_* is the surface friction velocity; κ is von Karman's constant; z_d is the zero-plane displacement; and z_0 is the surface roughness length.

The wind profile calculated from the power-law in Equation (3) and the logarithmic-law in Equation (4) demonstrates that, given the reference wind speed, the only parameter determining the wind speed at height z is the surface roughness conditions. In ASCE 7-22 (2022), surface roughness is categorised by terrain categories. Consequently, the wind speed at reference height becomes a critical input parameter in the development of wind fragility models for structures. However, extensive research has shown that for a given wind speed at reference height (V_r) , the wind profile is influenced by multiple parameters such as gust factor, turbulence intensity, and turbulence length scale (Kwon & Kareem, 2009; Q. S. Li et al., 2010; Snaiki & Wu, 2018). To address these uncertainties, an advanced numerical weather prediction (NWP) model, the Weather Research and Forecasting (WRF) model (Skamarock et al., 2019), is proposed in atmospheric science.

The WRF model is a numerical weather prediction system with a comprehensive description of atmospheric physics that involves the land-surface process, turbulence and vertical mixing, diverse radiation, and cloud models (WRF). The WRF can generate meteorological field data at high time frequencies (less than hourly) with a terrain resolution of less than 1 km (Xue et al., 2020). Because of the highresolution hurricane wind field information, the wind profiles obtained from the WRF can represent spatial and temporal variations of the winds in a region instead of being described by a unique distribution (Constantinescu, Zavala, Rocklin, Lee, & Anitescu, 2011).

In this research, the WRF model is utilised to simulate Hurricane Harvey by using data collected from the NCEP GFS FNL (National Centres for Environmental Prediction Global Forecast System Final Analysis) and the MODIS (Moderate Resolution Imaging Spectroradiometer). The data collected from NCEP GFS FNL is designed with a grid at a $27.8 \,\mathrm{km} \, imes \, 27.8 \,\mathrm{km}$ horizontal resolution. The WRF model, a mesoscale numerical weather prediction system, can downscale the NCEP GFS wind profiles to a high resolution of less than 1 km horizontal resolution. This study utilises WRF simulation data from 25th of August to 27th of August, with a one-hour time interval. Figure 2 illustrates the complexity of wind profiles in realistic hurricanes by comparing the wind profiles obtained from the WRF model to those derived using the power-law method, with a reference height wind speed taken as 40 m/s. The wind profiles from the WRF model encompass a wider wind speed range and retain the wind speed variations over height, as shown in Figure 2(a). The wind profile in log-log space, depicted in Figure 2(b), where the slope represents the surface roughness coefficient in Equation (3), reveals the strong nonlinearity between wind speed and height, thereby indicating that the power-law is not sufficient to fully characterise the complexity of the wind profile in a hurricane.

2.1.2. Turbulent wind characteristics

The turbulent wind speed is computed from the sampled wind profile, in which the spatial and temporal correlation is considered. Based on the Shinozuka theory (Shinozuka & Deodatis, 1991), the turbulent wind speed $\{v_1(t), v_2(t), \ldots, v_n(t), \ldots, v_$ $v_{np}(t)$ at time t is:

$$v_k(y_k, z_k, t) = \sqrt{2(\Delta \omega)} \sum_{m=1}^k \sum_{l=1}^N |H_{jm}(\omega_{ml})| \cos(\omega_{ml}t)$$

$$-\theta_{km}(\omega_{ml}) + \Phi_{ml}$$

$$\omega_{ml} = (l-1)\Delta \omega + \frac{m}{N} \Delta \omega, l = 1, 2, \dots, N$$
(6)

where N is an arbitrarily large positive number; k is the number of simulation points, k = 1, 2..., np; $\Delta \omega = \frac{\omega_{up}}{N}$, the frequency increment; and ω_{up} is the cut-off frequency, that is, when $\omega > \omega_{up}$, $S(\omega) = 0$; Φ_{ml} is uniformly distributed random phase angle in $[0, 2\pi]$. θ_{km} is the $H(\omega)$ phase angle. In engineering, $S(\omega)$ and $H(\omega)$ are real matrices, thus $\theta_{km} = 0$, while H_{jm} is the $S(\omega)$ Cholesky decomposed matrix as in Equation (5):

$$S(\omega) = H(\omega)H^*(\omega)^T \tag{7}$$

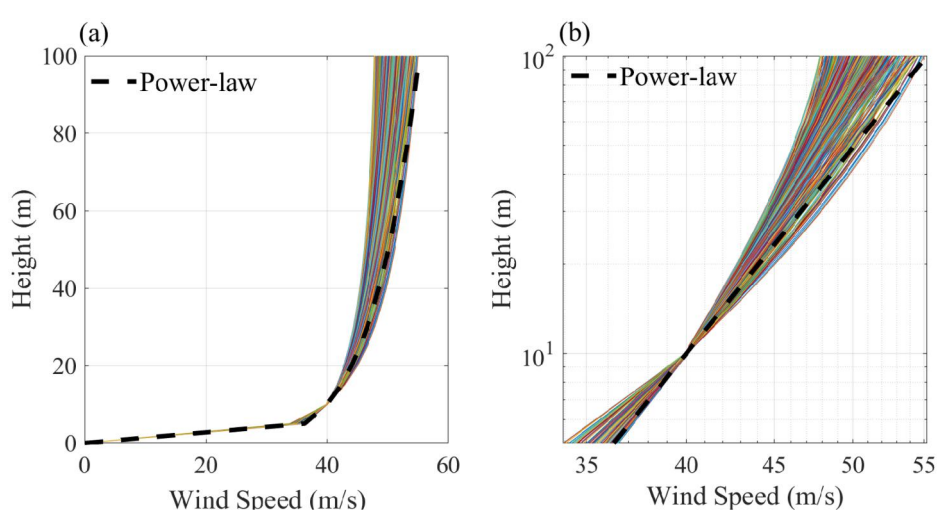


Figure 2. Wind profile comparison between WRF model and power-law: (a) wind profile in cartesian space; (b) wind profile in log-log space.

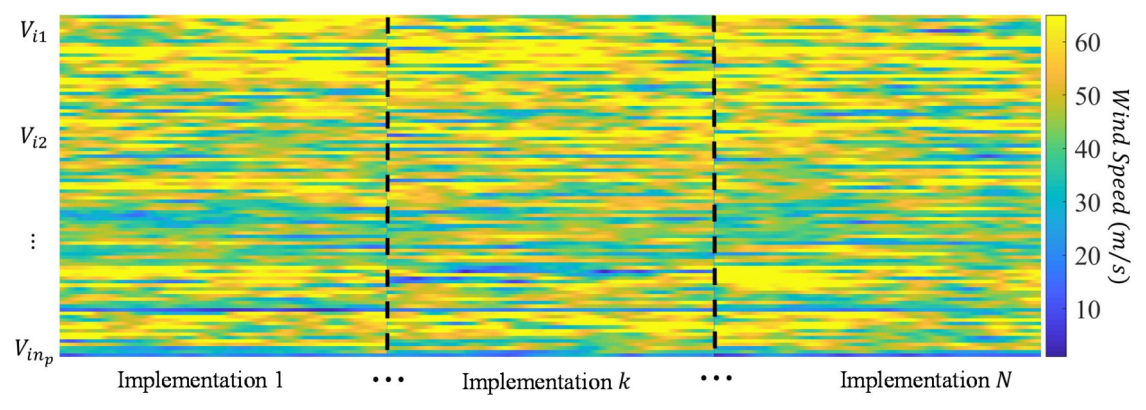


Figure 3. Illustration of the generated dynamic wind speed time-history stochasticity among different implementations and the wind speed variations at each node for a single implementation given a determined wind profile.

in which, the fluctuating wind spectral density matrix $S(\omega)$ is calculated from Davenport auto-correlation spectrum and cross-correlation spectrum (Davenport, 1961).

To account for the stochastic nature of the dynamic wind loading imposed on the structure, Figure 3 depicts the generated dynamic wind speed time history for the structure shown in Figure 12, across three different implementations with the same wind profile. The patterns of wind speed intensity in Figure 3 vary among the implementations, indicating that the turbulent wind speed component, as defined in Equation (7), influences the dynamic wind speed time history. Furthermore, for each dynamic wind speed implementation, the pattern of wind speed time history differs among nodes due to the spatial correlation of wind speed, which is markedly distinct from seismic loadings.

2.2. Transmission tower-line structure analysis tool

Accurately estimating power infrastructural damage and failure conditions during a hurricane event requires a highfidelity, computationally efficient transmission tower-line structure model. The nonlinear system, subject to wind loadings and transmission line vibrations, exhibits strong tower-line coupling, making accurate modelling a challenge (Xie, Cai, & Xue, 2017). Although finite element models (FEMs) of coupled transmission tower-line systems under wind loading have been widely studied, evaluating these models on a regional scale involving tens of thousands of transmission towers is computationally prohibitive.

To overcome this limitation, the fragility curve of the transmission tower, considering transmission tower-line coupling, is extensively used (Fu, Li, Tian, Wang, & Cheng, 2019; Tian, Zhang, & Fu, 2020; Xue et al., 2020). However, when applied to regional-scale power network reliability analysis, the pre-defined limit states significantly influence the generation of fragility curves. As a result, researchers have paid considerable attention to increasing FEM fidelity by considering uncertainties in material and geometry, component buckling, and joint models in the literature (Ma, Christou, & Bocchini, 2022; Ma, Khazaali, & Bocchini, 2021; Mohammadi Darestani, Shafieezadeh, & Cha, 2020; J. Wang, Li, Fu, & Li, 2021).

However, there are limitations to using fragility curves for regional power network resilience analysis. Firstly, the fragility function only provides the probability of infrastructural responses exceeding a predefined limit state, without offering time histories or other high-resolution information that could be used to define additional limit states. Secondly, the fragility curves are developed based on wind profiles that adhere to theoretical power- or logarithmic-law assumptions. These theoretical fragility curves consider only the basic wind speed at reference height as input, without accounting for variations in wind profiles over height. Consequently, the tower failure probability is often inaccurately calculated (and often too conservative).

2.3. Proposed structure analysis tool and wind profiles sampling methods

To address the limitations discussed in Sections 2.1 and 2.2, this paper proposes a surrogate model trained with realistic wind profiles as an infrastructure analysis tool. The objective of the developed surrogate model is to enable prompt and accurate predictions when the transmission tower-line structure is subjected to hurricane wind loading. Therefore, the representativeness of the dynamic wind loadings affects both the surrogate model prediction accuracy and robustness. Neural network models are widely utilised for solving sequence-to-sequence problems.

Among these models, Recurrent Neural Networks (RNNs) are preferred as they can manage functions involving recurrence (Goodfellow, 2016). However, RNNs encounter gradient vanishing problems while optimising model parameters, which restricts their ability to predict high nonlinearity and time-dependent dynamic problems (Goodfellow, 2016). To solve this problem, Hochreiter and Schmidhuber (1997) developed the Long Short-Term Memory (LSTM) model that incorporates gated features. These gated features enable the LSTM model to exploit current input-output local relations and explore both current and previous input-output globally. As a result, the LSTM model can maintain nonlinearity and time-dependence in time series.

To develop an effective surrogate model capable of predicting the accurate dynamic time history of the transmission tower-line system on a regional scale, the training dataset must be representative and align with realistic loading conditions. Given the broad and complex nature of wind loading across the entire region, it involves two types of variations: wind profile variation and turbulent dynamic wind stochasticity. As mentioned earlier, the wind loading in the entire region can be divided into the mean wind speed, which is dominated by the wind profile and the turbulence wind component. The hypothesis guiding the surrogate training is that the turbulent wind characteristics are implicitly embedded in each training sample, and the representativeness of training wind profiles predominates the quality of the surrogate model.

The Weather Research and Forecasting (WRF) model generates millions of high-resolution regional wind profiles that cannot be adequately described by empirical engineering models. For example, in the Hurricane Harvey WRF model, the mean wind speed ranging from [30m/s, 40m/s] at a height of 10 m encompasses over 200,000 wind profiles. It is impractical to use all these wind profiles to train the surrogate model. Therefore, appropriate sampling strategies must be employed to infer and extract the most representative wind profiles.

With respect to the wind profiles in the WRF model, they exhibit unique physical, mathematical, and statistical characteristics. Physically, a realistic wind profile can be approximated using a power-law or logarithmic-law function, with varying parameters along its height. To identify representative samples, a law-based sampling method can be applied. Mathematically and statistically, each wind profile can be viewed as high-dimensional data, where each dimension corresponds to a specific height. To partition the data, the k-medoids clustering method, which has been utilised in various domains, is applied (Likas, Vlassis, & Verbeek, 2003; Tzortzis & Likas, 2009). One potential method for sampling is random sampling, which does not require any prior knowledge about the wind profiles. In the processing of conducting this method, all wind profiles in the WRF model have an equal probability of being selected, making it a

benchmark sampling method for assessing the accuracy and robustness of other proposed sampling methods. Apart from random sampling, three other methods have been employed to build the surrogate model: (1) physics-guided sampling based on the power-law, (2) k-medoids sampling, and (3) modified statistical sampling.

3. Methodology

3.1. LSTM architecture

The LSTM model comprises an input layer, multiple LSTM layers, fully connected layers, and output layers, as illustrated in Figure 4. The input layer is dimensioned at $m \times$ $n \times p$, where m is the training size, n is the total number of time steps, and p equals the number of features, corresponding to the number of nodes in the numerical model. For each training sample, the sequence $X = [x_1, x_2, x_3, \dots, x_n]^T \in$ $\mathbb{R}^{n \times p}$ is sequentially fed into *n* LSTM cells. Consequently, one LSTM cell processes one time-step with p features, $\mathbf{x}_t \in \mathbb{R}^p$. Figure 5 clarifies the detailed operation of the LSTM at time t in layer l, where f_t^l , i_t^l , and o_t^l symbolize the forget state, input state, and output state respectively. The cell state and hidden state connect the information stream from time t-1 and t, depicted as continuous horizontal lines in Figure 5. The mathematical representations of these variable relationships are:

$$f_t^l = \sigma \left(W_{xf}^l \mathbf{x}_t + W_{hf}^l \mathbf{h}_{t-1}^l + \mathbf{b}_f \right)$$
 (8)

$$\mathbf{i}_{t}^{l} = \sigma \left(\mathbf{W}_{xi}^{l} \mathbf{x}_{t} + \mathbf{W}_{hi}^{l} \mathbf{h}_{t-1}^{l} + \mathbf{b}_{i} \right)$$
(9)

$$\tilde{\boldsymbol{c}}_{t}^{l} = \tanh\left(\boldsymbol{W}_{xc}^{l}\boldsymbol{x}_{t} + \boldsymbol{W}_{hc}^{l}\boldsymbol{h}_{t-1}^{l} + \boldsymbol{b}_{c}\right)$$
(10)

$$\boldsymbol{o}_{t}^{l} = \sigma \left(\boldsymbol{W}_{ro}^{l} \boldsymbol{x}_{t} + \boldsymbol{W}_{ho}^{l} \boldsymbol{h}_{t-1}^{l} + \boldsymbol{b}_{o} \right) \tag{11}$$

$$\boldsymbol{c}_{t}^{l} = \boldsymbol{f}_{t}^{l} \cdot \boldsymbol{c}_{t-1}^{l} + \boldsymbol{i}_{t}^{l} \cdot \tilde{\boldsymbol{c}}_{t}^{l}$$
 (12)

$$\boldsymbol{h}_{t}^{l} = \boldsymbol{o}_{t}^{l} \cdot \tanh\left(\boldsymbol{c}_{t}^{l}\right) \tag{13}$$

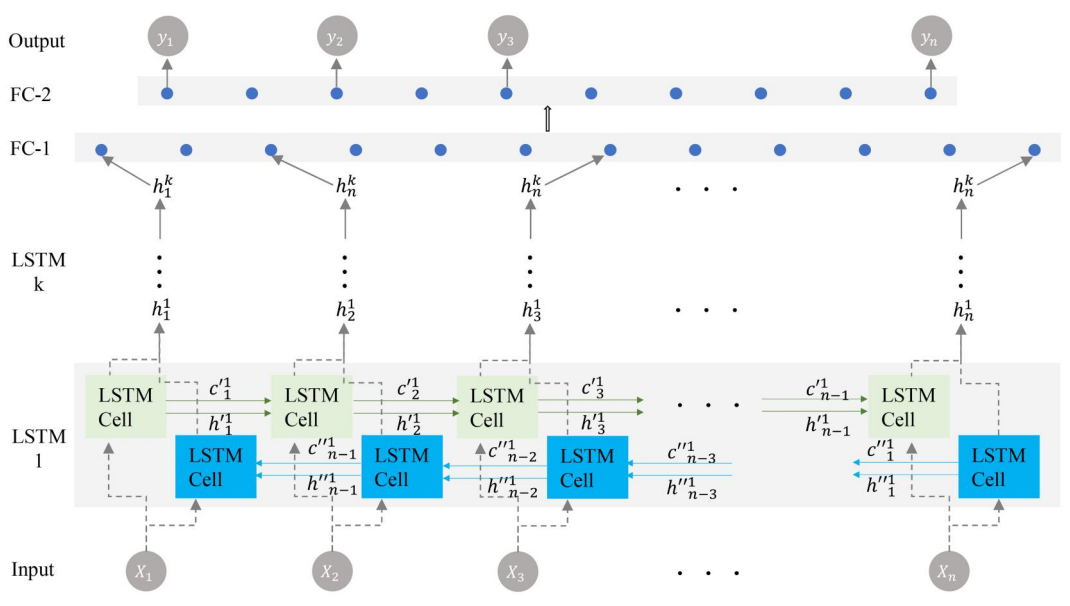


Figure 4. Multi-layer LSTM architecture for the full sequence-to-sequence modelling.

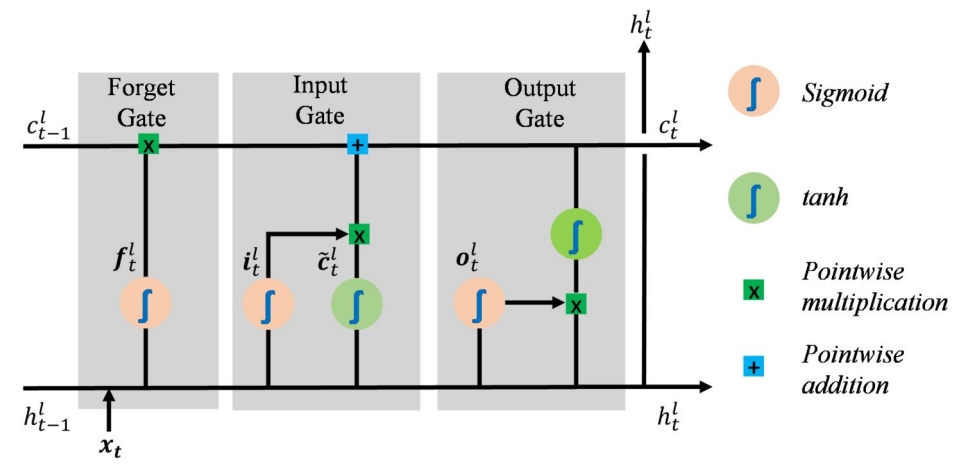


Figure 5. The diagram of the LSTM cell in layer I at time step t.

where, W_{x*} and b_* represent the weight matrix and bias vector; c_{t-1}^l and h_{t-1}^l are the cell state and hidden state output that contains previous time step information; c_t^l and h_t^l are the cell state and hidden state output in the current state; \tilde{c}_t^l represents the candidate values. The values in the forget gate f_t^l and input state i_t^l are in the range between [0, 1] to indicate the contribution of the previous information stream and current input values to the current state.

From Equation (12), the LSTM cell achieves long-term dependence by using the forget gate to control the extent of previous information required and using the input gate to adjust the amount of current input candidate values information. Additionally, a sample input-output preprocessing technique proposed by Zhang et al. (2019) is used to increase the prediction accuracy and reduce the computational time. Generally, the input sequence for one sample is $X = [x_1, x_2, x_3, \dots, x_n]^T \in \mathbb{R}^{n \times p}$ and $y = [y_1, y_2, y_3, \dots, y_n] \in$ $\mathbb{R}^{n\times q}$. The proposed method rearranges the input data X in a stacked size w as a new input vector to the LSTM cell. Therefore, the new input $X' = \{[x_1, x_2 \cdots, x_w], [x_{w+1}, x_{w+2} \cdots, x_{2w}], \cdots, [x_{n-w+1}, x_{n-w+2} \cdots, x_n]\}^T$ is fed into the LSTM network. The optimal choice of stack size is based on the sampling frequency and characteristics of the input training sample; hence it is considered a hyper-parameter in the surrogate model.

3.2. Wind profile sampling methods

3.2.1. Power-law-based sampling

The power-law-based sampling (PLS) method adopts a physics-based approach to generate wind profiles. This method calculates the wind speed at different heights using the power-law equation, which is influenced by the surface roughness coefficient and the basic wind speed at the reference height. In the power-law-based sampling approach, the surface roughness coefficient is selected uniformly between the lower and upper bounds defined in ASCE 7-22 (2022). This method is considered offline, indicating that the chosen training profile inputs are not event-specific, allowing the surrogate model to be trained offline before the occurrence of the wind event. The PLS algorithm can generate a set of representative wind profiles, enabling the training of a surrogate model to predict the accurate dynamic time history of the transmission tower-line system on a regional scale.

3.2.2 K-medoids clustering sampling

K-medoids clustering is a statistical sampling method similar to k-means clustering, wherein the representative object, known as the medoid within each cluster, is chosen from the dataset (Kaufman, 1990). Thus, in the k-medoids clustering method, the centroid of each group is constrained to the actual data samples. With this medoid feature, kmedoids clustering exhibits less sensitivity to outliers compared to k-means clustering (Park & Jun, 2009). Within each group, the k-medoids clustering method seeks to minimise dissimilarity by defining distance functions such as Euclidean. Consequently, the objective function can be expressed as:

$$Loss = argmin \sum_{i=1}^{k} \sum_{s_i \in C_i} f(s_j, m_i)$$
 (14)

where k is the total number of sets; s_i is the sample in the data set; C_i is set i; m_i is the medoids in set C_i ; and f is the distance function. The minimum value of Equation (14) is determined by the predefined criteria.

From Equation (14), for each update, the distance between m_i and the remaining samples needs to be calculated. Hence, with a substantial number of samples, the kmedoids method is computationally intensive. To alleviate the computational burden, a modified k-medoids clustering method has been proposed. Among these, a simple and fast k-medoids algorithm by Park and Jun (2009) is the most widely used and available in many computation libraries (MATLAB, SK-LEARN). Consequently, in this paper, the kmedoids algorithm based on Park et al. (Park & Jun, 2009) is utilised. After the dataset has been partitioned into k sets, samples are randomly selected in each set to meet the training sample number requirement. The partitioning of the wind profiles using k-medoids clustering by visualising the wind speed in the selected nodes is shown in Figure 6. The

stratified patterns in this figure demonstrate the distancebased functionality in KMCS.

3.2.3. Modified statistical sampling

Statistical sampling, also known as systematic sampling, is a probabilistic sampling method aiming to cover as wide a sample space as possible (Yates & Thornton, 1948). The original systematic sampling method involves ordering the samples and partitioning the sequence into K intervals. A random sample is selected as the seed point in the first interval, and the samples in the remaining intervals are chosen at a fixed stride from the seed sample. This sampling method can work well for data with the same distribution property in each interval but may fail if the data have different distributions in each range. A modified systematic sampling method is proposed in this research to expand its application. The mean value u and the standard deviation σ of the wind speed at each height are calculated as the metrics, which are subsequently used to derive the sampled data as follows:

$$wp = (V_L - \mu) + d*\sigma \tag{15a}$$

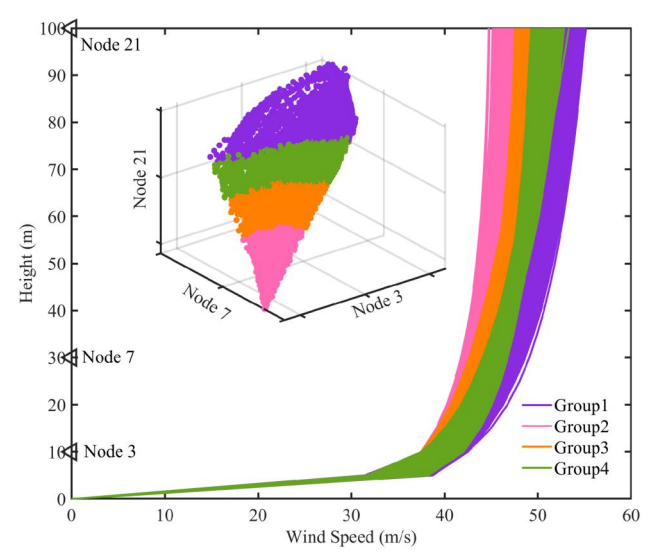


Figure 6. Visualization of k-medoids clustering based sampling on the regional wind profiles: (a): selected nodes wind speed distribution; (b) clustered wind profiles.

$$d = V_L : \frac{V_R - V_L}{N} : V_R \tag{15b}$$

where wp is the sampled wind profile; d is the stride; V_L is the lowest wind speed; V_R is the highest wind speed; and N is the number of samples The proposed method remains the same as the original systematic sampling if the wind speed follows a uniform distribution. However, if the wind speed distribution is not uniform, Equation (15) allows for adjustments in the sampling to account for the wind speed distribution at each height while still covering a wider range of wind speeds. As the wind profile is a high-dimensional data that changes with height, the modified systematic sampling is performed at each predefined height. Then, the wind speeds are sequentially sampled and combined at each height to generate the profiles.

The procedures to implement the modified systematic sampling method can be illustrated in Figure 7. For the wind profiles in a region, first, apply Equation (15) to form the speed vector at each height into N points; then, select the i_{th} point at each height to assemble the wind profile. In Figure 7, wp_i is the i_{th} generated wind profile; $V_{[h_i,h_i,h_k]}$ is the wind speed at the corresponding height; and h_n is the total number of wind profile heights.

4. Performance assessment of the surrogate models

The sample cases used to evaluate the performance of the developed surrogate model are obtained from the power infrastructure performance simulation testbed during Hurricane Harvey. The wind profiles are extracted from the WRF model in the Texas region. According to the transmission tower-line fragility analysis, the fragility curve of the transmission tower-line system is a function of the mean wind speed, which represents a wind speed range around it. In this paper, the wind profiles in the Texas Region are divided into 12 groups based on the 10 m high wind speed, ranging from 15 m/s to 70 m/s with 5 m/s intervals (Xue et al., 2020). A surrogate model can be developed for each group. The wind profiles with a wind speed at 10 m in the range of 40 ± 2.5 m/s during Hurricane Harvey are adopted as prototypes to investigate the performance of the surrogate model.

In regional power system resilience analysis, transmission towers are often grouped into units with identical designs at

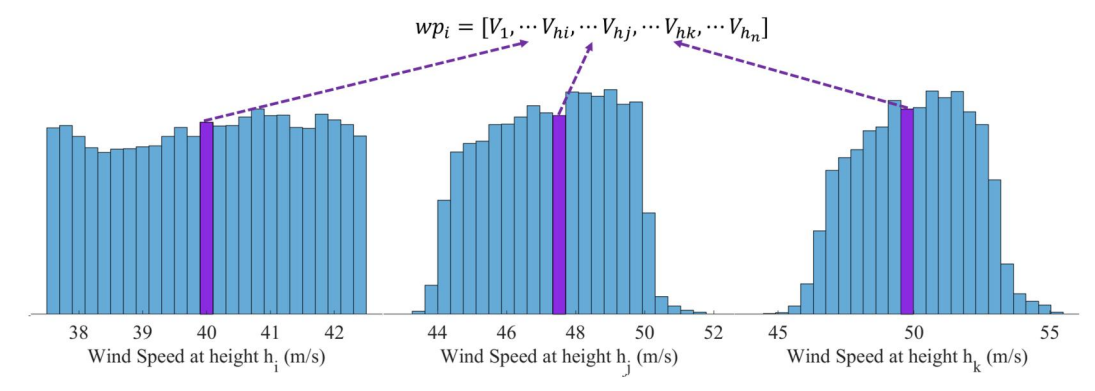


Figure 7. Visualization of modified systematic sampling on the regional wind profiles. At each height, the ith wind speed can be used to form the wind profile wpi.

various locations (Panteli, Pickering, Wilkinson, Dawson, & Mancarella, 2017). Therefore, only a single unit of transmission tower model is required for proof of concept. However, it is necessary to consider the coupling effects between the transmission tower and line in power system resilience analysis (Xue et al., 2020). In this paper, two transmission towerline structure configurations are modelled in OpenSees platform (Mazzoni, McKenna, Scott, & Fenves, 2006). The transmission tower is modelled by using the elastic beam-column elements with steel01 uniaxial bilinear steel material; the transmission line uses corotational truss element with initial stress material. The geometric nonlinearity is considered by taking the corotational geometric transformation. Hence, for the proposed transmission tower-line structures, both the material and geometric nonlinearity are considered.

In this study, the LSTM surrogate model is used to predict the tower tip displacement time history, from which the maximum displacement can be utilized as a key indicator for assessing the fragility of transmission towers (Bi, Tian, Li, Ma, & Pan, 2023; Dikshit & Alipour, 2023; J. Wang, Li, Fu, Dong, & Sun, 2022). This approach primarily focuses on the global response of the tower and does not specifically address the local failure mechanisms of the tower. The failure of transmission towers is commonly dominated by member buckling, which leads to structural instability (Ma et al., 2021). Owing to the high redundancy of the tower and complex loading conditions, there are many possible failure modes (Natarajan & Santhakumar, 1995). This complexity necessitates a comprehensive approach that includes detailed structural inventories and an in-depth analysis of element-level buckling.

However, the dynamic response of the tower tip displacement can indirectly reflect local element behaviours. This relationship can be obtained by comparing the buckled elements in the nonlinear pushover analysis and the dynamic responses. Furthermore, Fei, Zhou, Han, and Wang (2012) showed that the tower tip displacement is the primary indicator to reflect the global stability of the structure. Moreover, in the literature, tower tip displacement is widely used to indicate the global response of the transmission tower-line system (Xue et al., 2020; Xue & Ou, 2021; Xue et al., 2021; Zhu & Ou, 2021). Consequently, in this study, the node labelled 'target' in Figures 12 and 21 is selected to represent the nonlinear time history response of the structure. Hence, the dynamic wind loading time history of the wind simulation nodes in both x and v directions, and the displacement of the 'target' node are used as the inputoutput pairs for training the surrogate model.

Neural network hyperparameters significantly impact computational time and prediction accuracy. Therefore, identifying appropriate hyperparameters is crucial (Goodfellow, 2016). From the existing literature, with the provided training cases, the number of hidden units and LSTM layers are the two main hyperparameters that affect the prediction accuracy of the LSTM model (Xu, Lu, Cetiner, & Taciroglu, 2021; Xue & Ou, 2021). Hence, the effects of hidden units and LSTM layers on prediction accuracy are studied. Moreover, since the stacked input sequence is utilised to preprocess the samples, the influence of the stack size on the LSTM model is examined. The determined LSTM architecture is then used to compare the effects of different sampling methods. The surrogate model is trained with the determined hyperparameters, and accuracy and robustness are evaluated using the same unseen testing wind profiles with surrogate models trained by different sampling methods. The flowchart in Figure 8 illustrates the accuracy and robustness assessment of surrogate models trained with different sampling methods in the wind speed range of $40\pm2.5~m/s$.

4.1. Implementation of different sampling methods on regional wind loading conditions

In the previous section, four sampling methods are introduced: k-medoids clustering-based sampling (KMCS), random sampling (RS), power-law sampling (PLS), and modified systematic sampling (MSS). As depicted in Figure 8, the wind profiles for the Hurricane Harvey event are partitioned into training, accuracy, and robustness testing sets. The four proposed sampling methods extract the training and validation cases separately from the training wind profile database. The dynamic wind loadings are calculated based on the methods described in Section 3 by using the sampled wind profiles and are then fed into the structure model to obtain the target displacement.

The sampled wind profiles obtained using the proposed sampling methods are shown in Figure 9. All the sampled wind profiles cover the speed range of the wind profiles in the WRF model. However, the coverage area is slightly

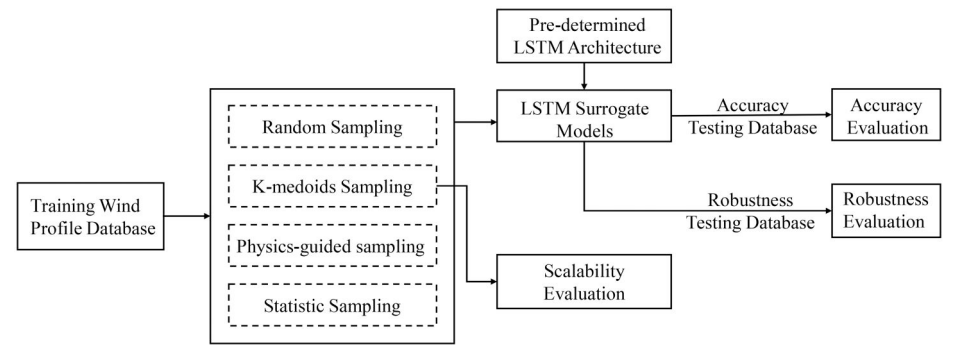


Figure 8. Flowchart of the surrogate model accuracy and robustness evaluation.

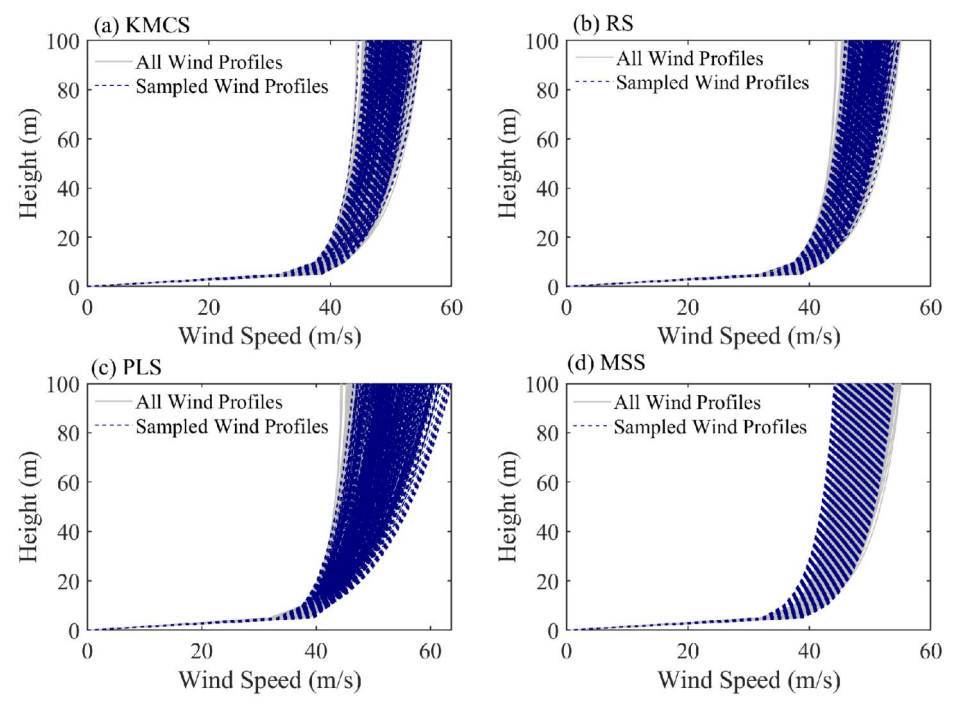


Figure 9. Different sampling methods sampled wind profiles illustration for training and validation.

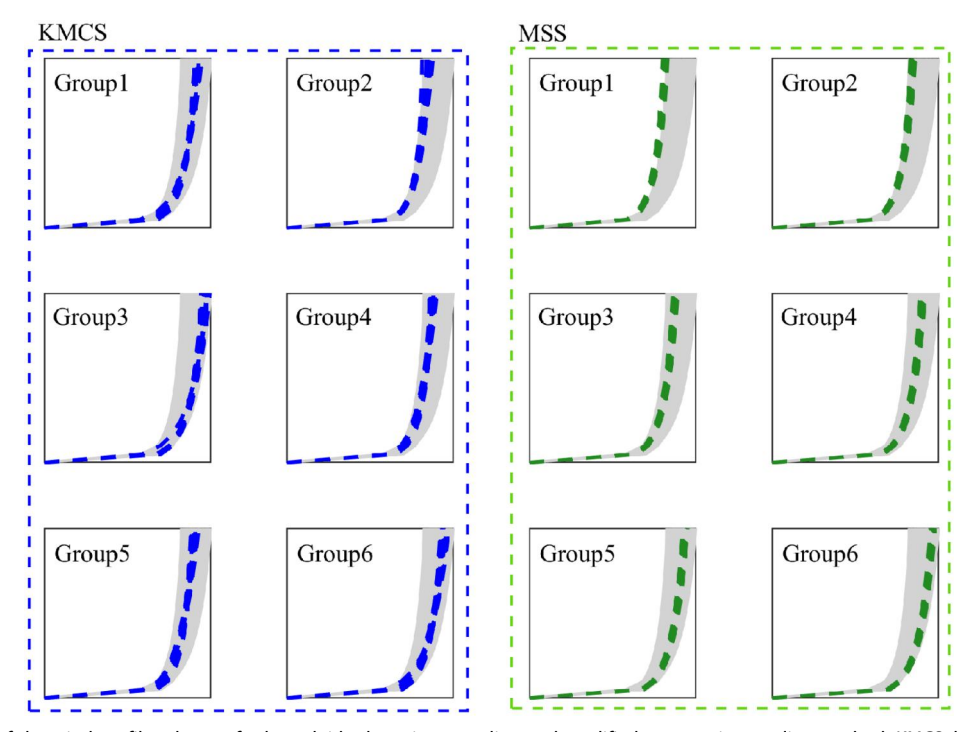


Figure 10. Illustration of the wind profiles clusters for k-medoids clustering sampling and modified systematic sampling method. KMCS: k-medoids clustering sampling method; MSS: modified systematic sampling method.

different for each method. Since the KMCS and RS methods extract the raw wind profiles, the sampled wind profiles are a subset of all wind profiles in the WRF model event pool. In contrast, the PLS method, which uses the surface roughness coefficients recommended by ASCE 7-22 (2022) for all terrain categories, has broader coverage than the numerical model wind profiles and can be considered event-independent. The MSS method automatically infers the wind speed

distribution at each height and assembles it in order, resulting in sampled wind profiles with similar coverage to KMCS and RS but more evenly distributed. Furthermore, since the KMCS and MSS methods cluster the wind profiles based on the defined distance metric, these two sampling methods should exhibit distinct patterns in each group. Figure 10 shows the wind profiles sampled in each group for these two methods.

4.2. Two-tower one-span transmission tower-line surrogate model

The two-tower one-span transmission tower-line model in this paper is based on the model discussed by Zhu and Ou (2021), where they detailed techniques for modelling transmission tower-lines. This model is employed as a test case in our study. Figure 12 displays the two-tower one-span model, the geometry of which is shown in Figure 11, and eight transmission lines, comprising six conductors and two ground wires. The lattice transmission towers are composed of A36 steel angles. The geometric and material properties of the conductors and ground wires are listed in Table 1. The wind loading simulation points are shown in Figure 12.

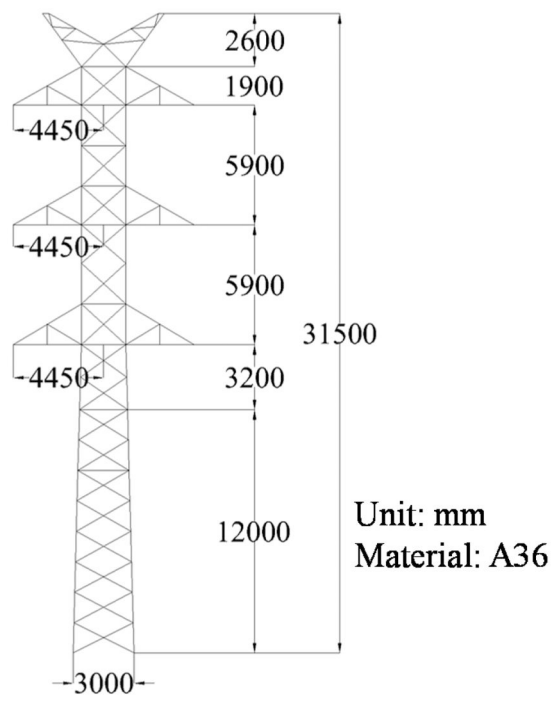


Figure 11. Transmission tower geometry.

4.2.1. Surrogate model accuracy evaluation

To compare prediction accuracy using different hyperparameter values, 300 training samples, 100 validation samples, and 100 testing samples were utilised. Wind profiles extracted from the Hurricane Harvey WRF model on the 26th of August at 04:30, with a basic wind speed in the range of 40 ± 2.5 m/s, are employed for this study. The findings indicate that the most proficient LSTM structure consists of six layers, each with 512 hidden units, and stacking the input sequence with four time-steps. This determined LSTM architecture is then used to compare the effects of different sampling methods.

Figure 13(a) depicts the distribution of RMSE for surrogate models trained using different sampling methods and training case numbers. The results indicate that the overall prediction accuracy of surrogate models increases with the number of training cases. The KMCS method exhibits the best prediction accuracy for all training case numbers, except for the surrogate model trained with 200 cases. In contrast, the MSS method has the worst prediction performance across all training case numbers. The KMCS method is particularly effective as it improves the training efficiency by up to 30% compared to the worst-performing MSS method. However, for the k-medoids sampling method, 100 training cases do not yield acceptable accuracy due to the stochastic nature of turbulent loading.

When trained with 400 cases, all the four proposed sampling methods have improved accuracies. Table 2 compares the relative differences in RMSE prediction at the mean and 75th percentile levels compared to the KMCS method. The MSS trained surrogate model shows a 10% larger RMSE prediction than the KMCS method at all accuracy levels. This may be because the MSS method sequentially

Table 1. Material and geometric properties of the ground wires, conductors, and insulator.

Component	Ground wire	Conductor	Insulator
Cross-section Area (m ²)	0.000329	0.000605	0.0908
Young's Modulus (Gpa)	78	67	100
Density (kg/m^3)	4602	1780	45.24
Sag (m)	2.9	3.7	\

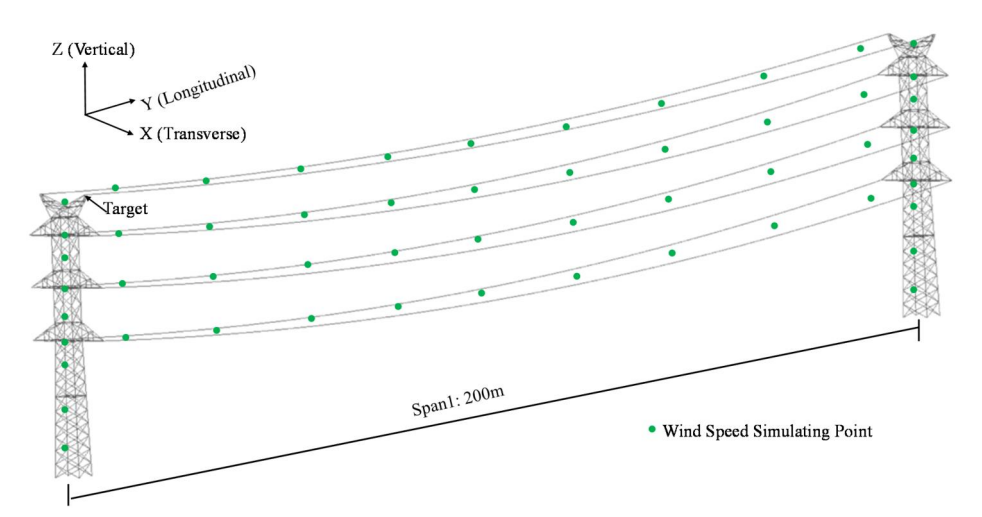


Figure 12. Two-tower one-span transmission tower-line model.

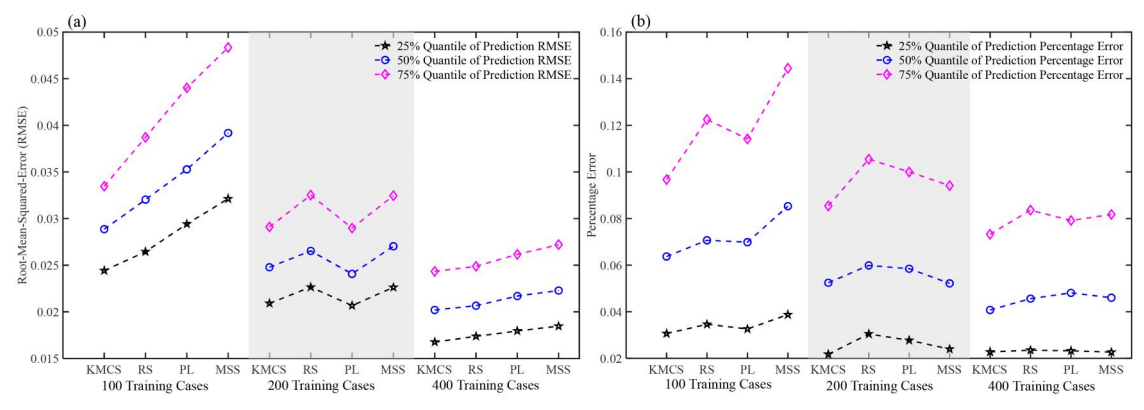


Figure 13. Comparison of the efficiency of the two-tower one-span surrogate model with different training sizes: (a) root mean square error; (b) maximum top displacement.

Table 2. RMSE of the four sampling methods trained two-tower one-span surrogate model prediction at mean and 75th quantile value for accuracy testing.

	Mean value		75th quantile value	
	Absolute value	Difference to KMCS (%)	Absolute value	Difference to KMCS (%)
KMCS	0.0202	0.000	0.0243	0.000
RS	0.0207	2.309	0.0249	2.248
PLS	0.0217	7.411	0.0262	7.520
MSS	0.0223	10.345	0.0272	11.797

assembles the wind speed at each height to generate the wind profile, resulting in a more restricted variation in the wind profiles. The physics-based PLS method trained surrogate model RMSE prediction is 7% larger than the KMCS trained surrogate models. Although the surface roughness coefficient takes values for all terrain categories in the PLS method, the sampled wind profiles are straight lines, as shown in Figure 2, and do not consider the variation of the wind profiles along the height. Therefore, the prediction accuracy of the PLS method trained surrogate model is relatively lower than that of the KMCS method.

As introduced in Section 4, when generating the transmission tower fragility curve, the peak tower top displacement in the predicted time history is generally chosen as the failure criterion (Xue et al., 2020). Therefore, the predicted peak displacement in the time history is another essential parameter to evaluate the accuracy of the developed surrogate model. The predicted tower top peak displacement comparison with the FEM for 100, 200, and 400 cases is shown in Figure 13(b). The results indicate that with more training cases, the surrogate models predicted tower top peak displacement discrepancy with the FEM is smaller. With 400 training cases, the KMCS trained surrogate model peak displacement is 7.33% different from the FEM at the 75th quantile. In Figure 14, the convergence rate of the predicted tower top displacement time history and the peak displacement are compared. It can be observed that the predicted response peak displacement converges faster than the displacement time history as the error difference between the prediction and target values in 200 cases and 400 cases are much smaller.

Statistically, when the training size increases to 400 samples, the difference between each sampling algorithm is not

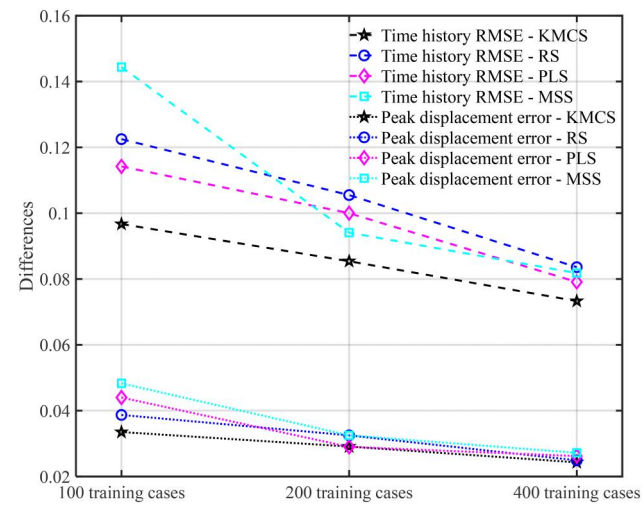


Figure 14. Comparison of the different sampling methods trained two-tower one-span surrogate model trained by 100, 200, and 400 cases convergence rate for time history and peak displacement prediction.

distinctive for both the time history and peak displacement value prediction. The RMSE indicator is critical for comparing the predicted and target displacement time history. To further enhance the accuracy analysis of the surrogate model predicted displacement time history, the cross-correlation coefficient between the predicted and target displacement time history from KMCS is shown in Figure 15(a), in which the cross-correlation coefficient is all higher than 0.8, referring to the high prediction accuracy. The comparisons of the predicted and target time history in Figure 15(b) (c), and (d) demonstrate the high fidelity of the trained surrogate model. Besides, the average computational time is 52s for all the surrogate models, significantly decreasing compared to the FEMs (Zhu & Ou, 2021).

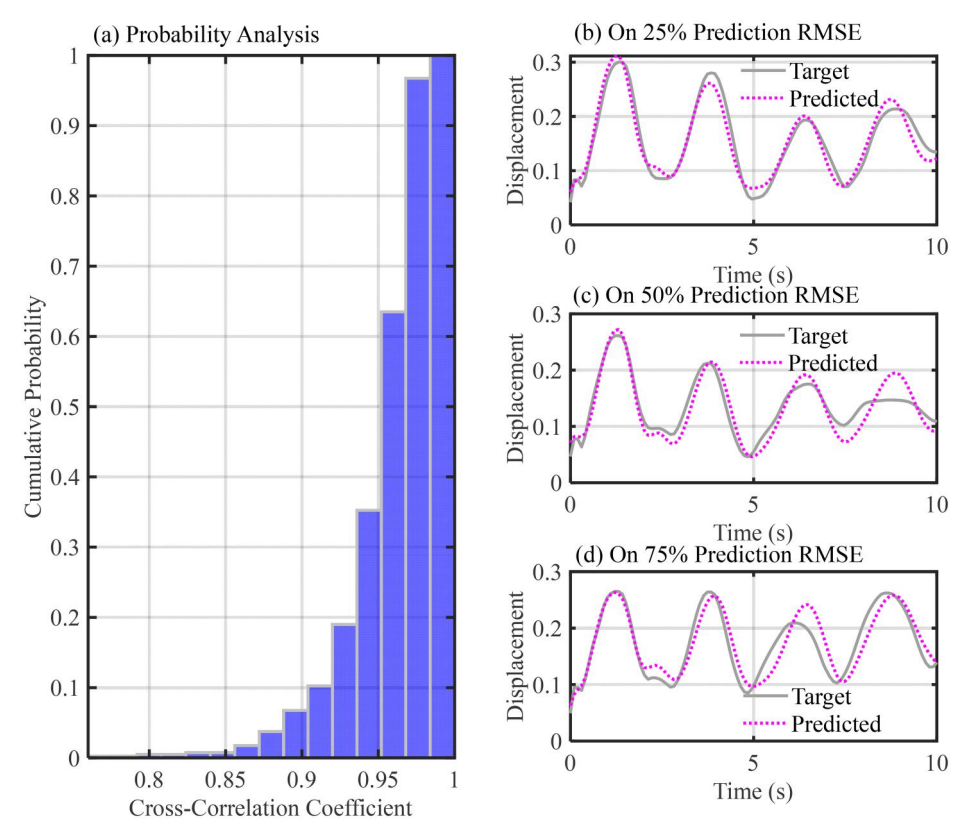


Figure 15. KMCS method trained two-tower one-span surrogate model prediction RMSE cumulative probability and the predicted time-history for accuracy testing.

4.2.2. Robustness assessment of the trained surrogate model

Wind profiles utilised for training and assessing surrogate models are extracted at the timestamp of 26th of August at 04:30, during the duration of Hurricane Harvey from 25th of August to 27th of August. Owing to the dynamic atmospheric conditions, such as humidity, temperature, and pressure gradient force variation, wind profile characteristics alter over time. Hence, evaluating the robustness of trained surrogate models at alternative timestamps is crucial to ascertain their proficiency. Moreover, as wind profiles within a hurricane encompass a vast geospatial region, assessing their geographical location is equally imperative to evaluate the robustness of the surrogate model. Therefore, to train the surrogate model effectively, it is essential to consider both the location and timestamp of wind profiles to evaluate the proficiency.

To assess the robustness of the trained surrogate model, wind profiles in the $40\pm2.5\,\text{m/s}$ range on the 26th of August at 08:30 were chosen, with 400 cases randomly selected from 40,000 wind profiles. Figure 16 depicts the predicted displacement time history RMSE for all sampling methods of the trained surrogate models. The mean and 75th percentile RMSE values of prediction for wind profiles on 26th of August at 04:30 and 26th of August at 08:30 are summarised and compared in Table 3. Based on the table, for the robustness testing of 400 cases on 26th of August at 08:30, the KMCS method is optimal, while the prediction accuracies of other models are comparable to the KMCS method. This finding supports the conclusion in

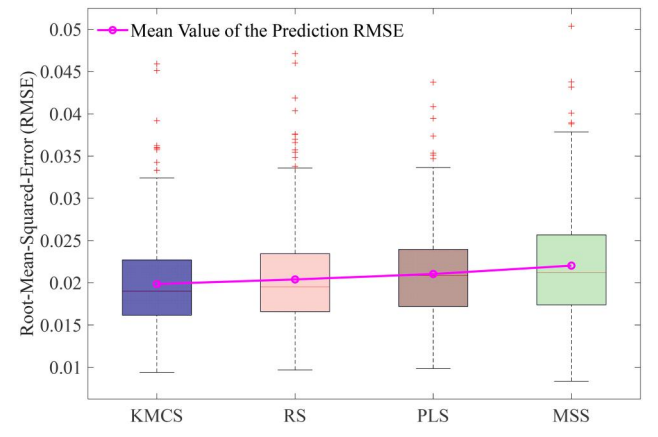


Figure 16. Robustness of the four sampling methods trained two-tower onespan surrogate model prediction RMSE on 26th of August at 08:30.

section 4.2.1. Thus, the trained surrogate model can accurately predict the transmission tower-line displacement response at different timestamps.

Apart from the wind profiles at the timestamp 26th of August at 04:30 and 26th of August at 08:30, the wind profiles in the range $40\pm2.5~m/s$ for the rest of the timestamps are gathered to select another 400 cases to investigate the robustness of the trained surrogate model in the sizeable geospatial wind profiles distribution. The 400 sampled wind profiles in Figure 17 show that the tested wind profiles filled the geospatial space of all wind profiles. To better illustrate the predicted tower displacement time history RMSE, four sections, as shown in Figure 18, are used to depict the evolution of Hurricane Harvey. In Figure 18, the mean values

Table 3. Developed two-tower one-span surrogate model robustness RMSE assessment on 26th of August at 08:30.

	Mean value		75% quantile value	
	26th of August at 04:30	26th of August at 08:30	26th of August at 04:30	26th of August at 08:30
KCMS-32	0.0210	0.0199	0.0243	0.0227
RS	0.0216	0.0204	0.0249	0.0234
PLS	0.0223	0.0210	0.0262	0.0239
MSS	0.0232	0.0220	0.0272	0.0257

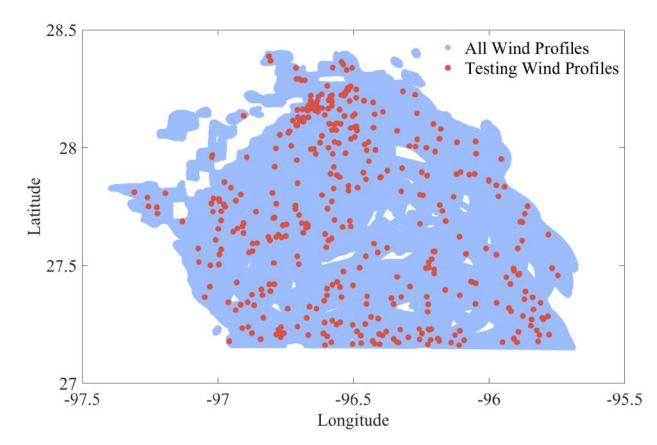


Figure 17. Robustness assessment sampled wind profile geospatial distribution.

of the RMSE indicate that the KMCS method is the smallest at all timestamps. Table 4 summarises the mean values and standard deviation of the RMSE for different sampling methods trained surrogate model. In this table, the KMCS method trained surrogate model predicted displacement time-history RMSE has both the smallest values and standard deviation. Other surrogate models can also produce satisfactory results. These small prediction RMSE mean values and standard deviation of trained surrogate models manifest their accuracy and robustness in regional power-system infrastructure analysis.

4.2.3. Scalability evaluation of the trained surrogate models

To assess accuracy and robustness in sections 4.2.1 and 4.2.2, wind speeds are restricted to a narrow interval of $40\pm2.5~m/s$ at a height of 10 metres. This interval represents a narrow wind speed range in Hurricane Harvey and thus may not fully encapsulate the entire spectrum of possible wind speeds. Furthermore, training a LSTM surrogate model for each wind speed interval can be time-consuming and may weaken the applicability of the model to regional scale problems. To circumvent this, a single LSTM surrogate model is developed to encompass the entire range of wind speeds pertinent for regional scale assessment of transmission tower-line structure response.

A total of 1500 wind profile cases are randomly selected to construct the model, which is trained by using 1125 cases and tested with 375 cases. To evaluate the performance of the model, an additional set of 140 wind profile cases is utilised for testing, which excluded the cases used for training and validating the surrogate model. To verify the scalability and accuracy of the LSTM surrogate model trained on the full wind speed range (LSTM-F), the LSTM model trained

on the $40\pm2.5~m/s$ wind speed range (LSTM-N) is also employed to predict the displacement time-history for the 140 testing cases. In Figures 19 and 20, the wind speed represents the mean wind speed for each interval within $a\pm2.5~m/s$ range.

As depicted in Figure 19, the displacement time-history prediction RMSE for LSTM-N forms a bowl shape, wherein the prediction RMSE is large when the wind speed interval deviates significantly from the trained wind speed of 40 ± 2.5 m/s. The bowl-shaped prediction RMSE arises because, when the wind speed at a 10-metre height diverges significantly from 40 ± 2.5 m/s, the mean wind force magnitude exerting on the structure differs from that within the 40 ± 2.5 m/s range. Furthermore, as outlined in section 3.2, the turbulence wind force is a function of the mean wind speed. Consequently, for mean wind speeds significantly different from 40m/s, both the prediction RMSE mean and standard deviation are larger than those observed around 40m/s. In contrast, the LSTM-F demonstrates small and consistent prediction RMSE values across the entire range of wind speeds, indicating its robustness and adaptability. Moreover, for the testing cases within the wind speed range of 40 ± 2.5 m/s, the mean RMSE prediction by LSTM-N is 0.0182, whereas for LSTM-F, it is 0.0148. This suggests that by incorporating variability in the training data, the LSTM surrogate model becomes more robust.

Figure 20 compares one predicted displacement time-history for each wind speed interval by LSTM-F and LSTM-N against the target displacement. In this figure, both the LSTM-F and LSTM-N displacement time-histories follow the same trend as the target displacement time-history. However, as LSTM-N is trained within a narrow wind speed interval, for wind speeds significantly different from $40\pm2.5~m/s$, the magnitude of the LSTM-N predicted displacement time-history diverges from the target. The LSTM-F predicted displacement time-history, on the other hand, is similar in both trend and magnitude when compared with the target, further illustrating its robustness and adaptability across a broader range of wind speeds.

5. Adapting the LSTM model and sampling methodology to a new transmission tower-line model configuration

In this section, an investigation is carried out into the consistency of the LSTM surrogate model in conjunction with the proposed sampling methods for predicting the response of transmission tower-line structures with various configurations. The objective is to evaluate the overall performance of the proposed surrogate model training methodology across

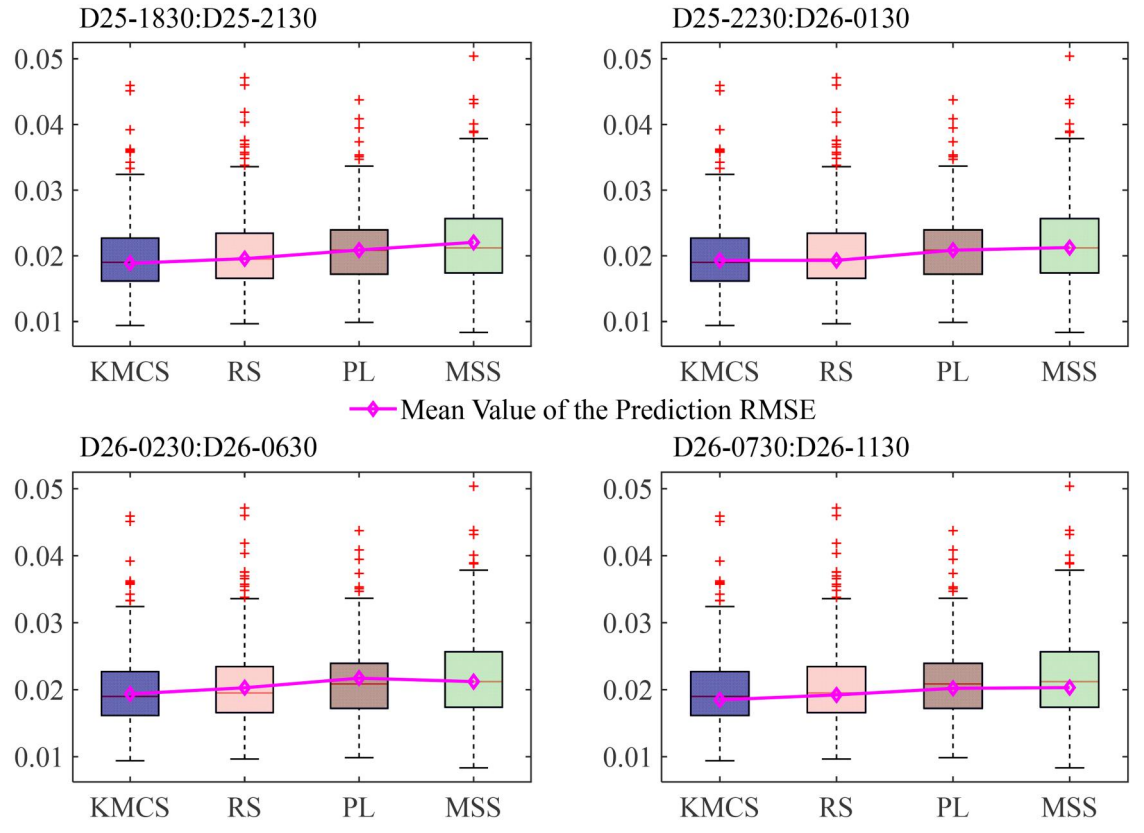


Figure 18. The prediction RMSE by different sampling methods trained two-tower one-span surrogate model distribution over time.

Table 4. The mean values of the RMSE at different time sections and the standard deviation for each sampling method trained two-tower one-span surrogate model.

Stacked Timestamp	Mean Value of Root-Mean-Squared Error (m)			
Stacked Timestamp	KMCS	RS	PLS	MSS
2017-08-25: 1830–2130	0.0189	0.0196	0.0209	0.0221
2017-08-25: 2230-0130	0.0193	0.0193	0.0209	0.0213
2017-08-26: 0230-0630	0.0194	0.0203	0.0217	0.0212
2017-08-26: 0730-1130	0.0185	0.0192	0.0202	0.0203
Standard Deviation	0.00041	0.00049	0.00062	0.00071

different transmission tower models. The one-tower two-span transmission tower-line model is widely utilised to simulate intermediate tower boundary conditions in transmission lines. In this setup, a single tower supports two spans, with each span comprising transmission lines connected to the tower *via* insulators. This arrangement accurately represents the interconnection between the tower and the transmission lines. Additionally, spring elements are used to appropriately model the end boundary conditions of the transmission lines at adjacent towers. Consequently, the one-tower two-span transmission tower-line model, as shown in Figure 21, is employed. The geometric details and materials of the insulators, ground wires, and conductors are listed in Table 1.

5.1. Investigation on the adaptivity of LSTM structure and hyper-parameters

As illustrated in Figure 21, the one-tower two-span transmission tower-line configuration exhibits increased

complexity due to the existence of a doubled number of lines highly exhibiting geometric nonlinear behaviour and the changes in line end boundary conditions. With the adoption of the two-span configuration, the nodes responsible for generating wind loading, as exemplified in Figure 21, increased to 156, in contrast to the two-tower one-span model, which utilises 98 nodes. This new structural model configuration increases the dimensionality feature for LSTM learning, which directly impacts the number of samples needed for optimal training as well as the architecture of the LSTM model. To validate such impact, the trained LSTM surrogate model for the two-tower one-span structure model is used to exam the necessities of re-tuning the hyper-parameters.

Figure 22 presents the trained one-tower two-span surrogate model prediction RMSE cumulative probability and the predicted time-history for accuracy testing using the twotower one-span surrogate model hyperparameters. From Figure 22(a), 40% of the predicted and target displacement time history cross-correlation coefficient is less than 0.8. Figure 22(b) (c), and illustrate the large discrepancy between the target and predicted displacement time history. Hence, with the new transmission tower-line structure configuration adapted, the LSTM surrogate model hyper-parameters need to be re-tuned. It is also observed that the training reaches its convergence with 1000 samples, consisting of 750 training samples and 250 validation samples. The one-tower two-span LSTM surrogate model hyper-parameter tuning finds that the most proficient LSTM architecture consists of seven layers, each with 512 hidden units, and four stacking sizes.

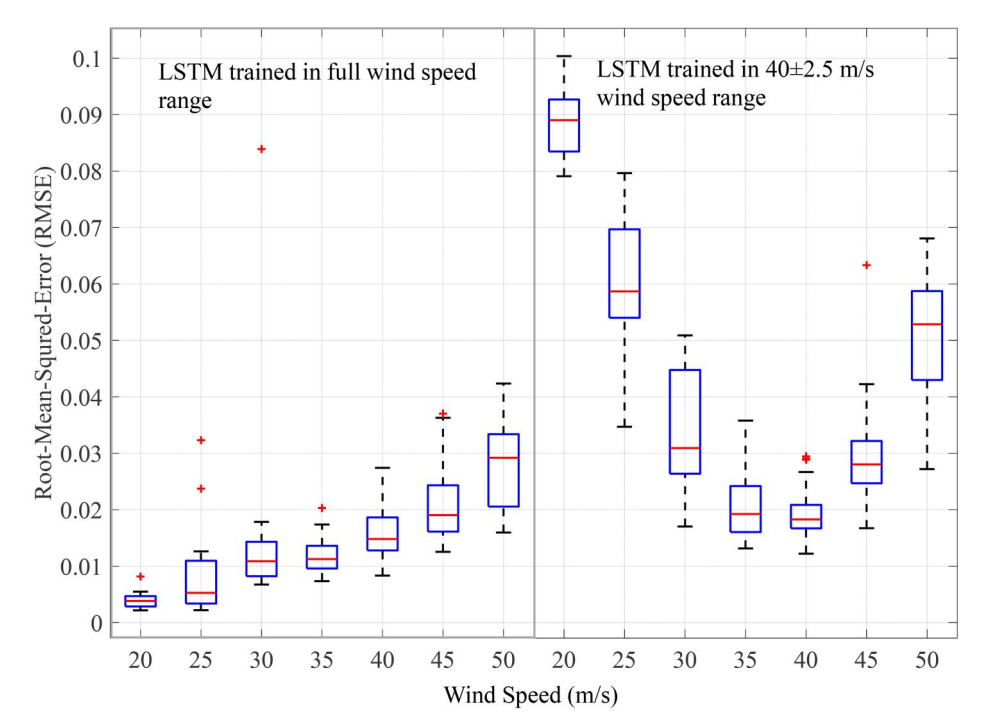


Figure 19. The prediction RMSE by two-tower one-span LSTM surrogate model trained by full wind speed range and 40±2.5 m/s.

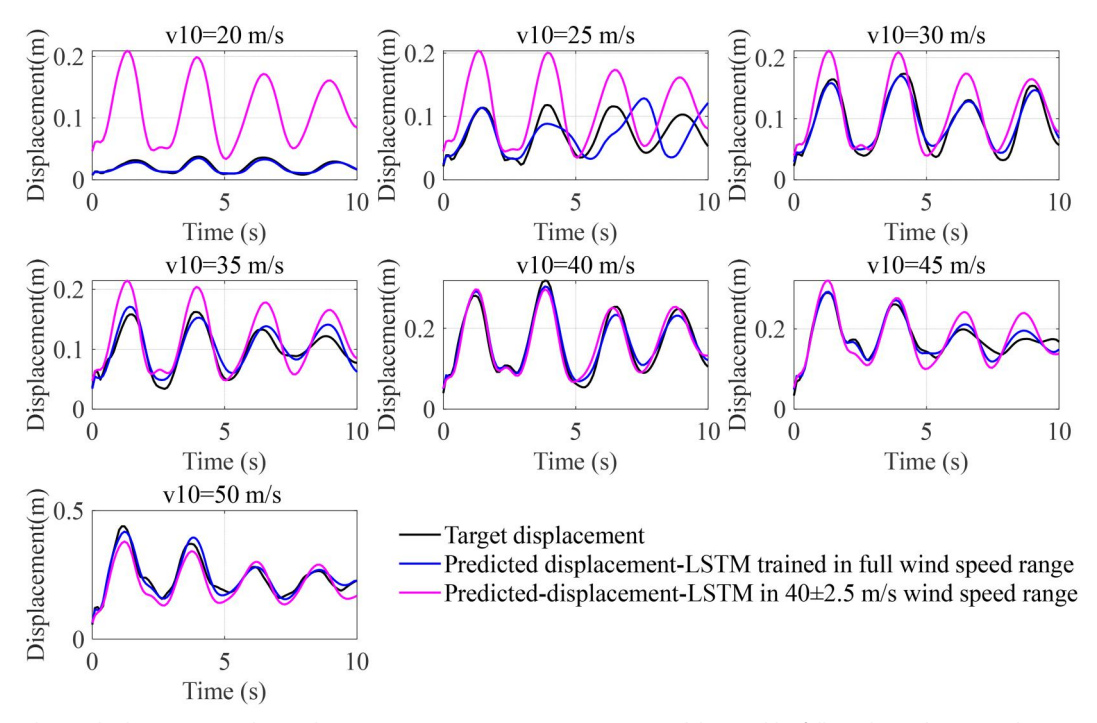


Figure 20. The prediction displacement time-history by two-tower one-span LSTM surrogate model trained by full wind speed range and $40\pm2.5~m/s$.

5.2. Investigation of LSTM accuracy performance with different sampling methods

Figure 23 displays the RMSE and percentage error for predicting peak displacement in comparison to the Finite Element Model (FEM) results. Additionally, Table 5 summarises the RMSE differences in predicted displacement time history with the target displacement time history, providing

mean and 75th percentile values, along with the relative differences compared to the K-medoids Clustering Sampling (KMCS) method across all 400 testing cases.

A comparison between Tables 5 and 2 reveals that the one-tower two-span surrogate model predicted RMSE is smaller than that of the two-tower one-span surrogate model. Furthermore, the predicted RMSE of Random

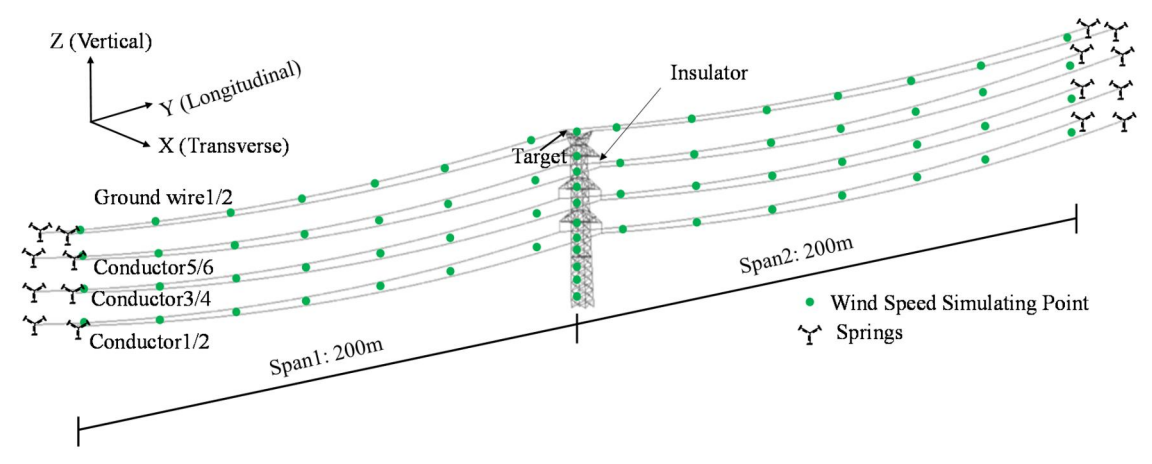


Figure 21. One-tower two-span transmission tower-line model.

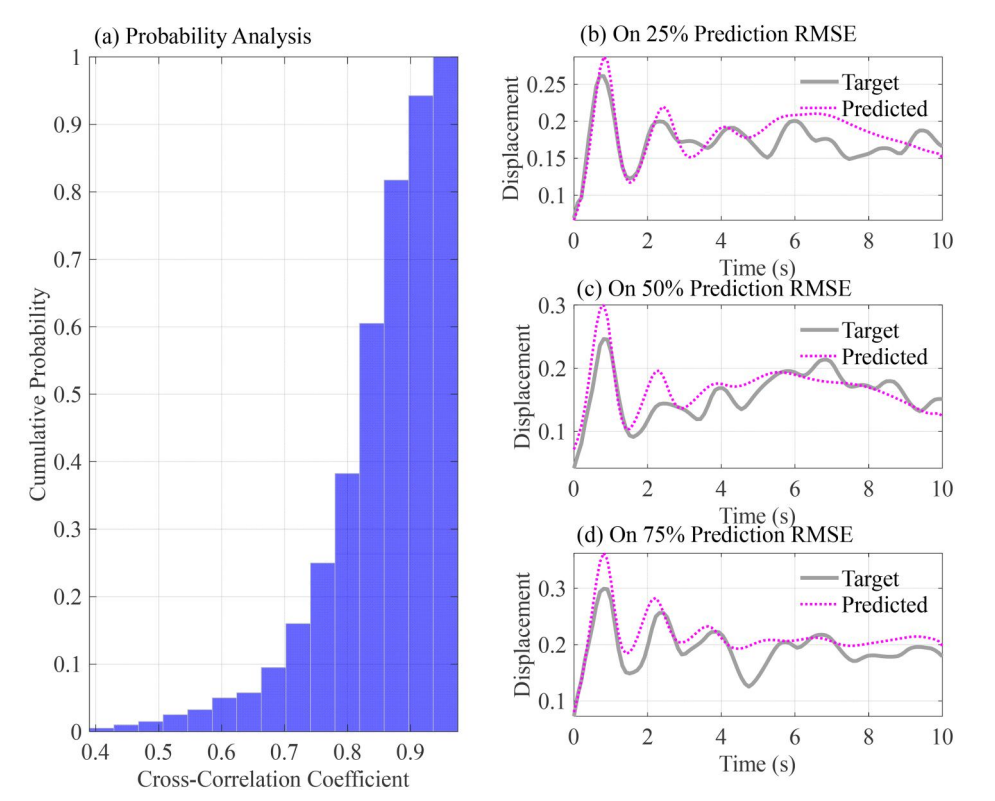


Figure 22. Trained one-tower two-span surrogate model prediction RMSE cumulative probability and the predicted time-history for accuracy testing using twotower one-span surrogate model hyper-parameter.

Sampling (RS), Power-Law-Based Sampling (PLS), and Modified Statistical Sampling (MSS) methods, in comparison to KMCS, is notably larger, exceeding 12.7% for the mean percentile and 17.4% for the 75th percentile. In contrast, for the two-tower one-span model, the maximum difference is 10.3% for the mean percentile and 11.8% for the 75th percentile. Figure 24 provides insight into the distribution of the cross-correlation coefficient and a visual comparison of the predicted displacement time history with the target. In Figure 24(a), it is evident that the predicted time history exhibits a strong linear correlation with the target. The results indicate that with the increased number of training cases, the surrogate model prediction accuracy increases. Additionally, the KMCS outperforms other sampling methods in all different numbers of training cases. Figure 25 shows the convergence rate of the surrogate model accuracy measurement metrics. It can be observed that the predicted response peak displacement converges faster than the displacement time history as the error difference between the prediction and target values in 700 and 1000 cases are much smaller.

5.3. Investigation of LSTM robustness performance with different sampling methods

As discussed in Section 2.1, evaluating the robustness of the trained surrogate model is crucial due to the spatial and temporal variability of hurricanes, which can result in

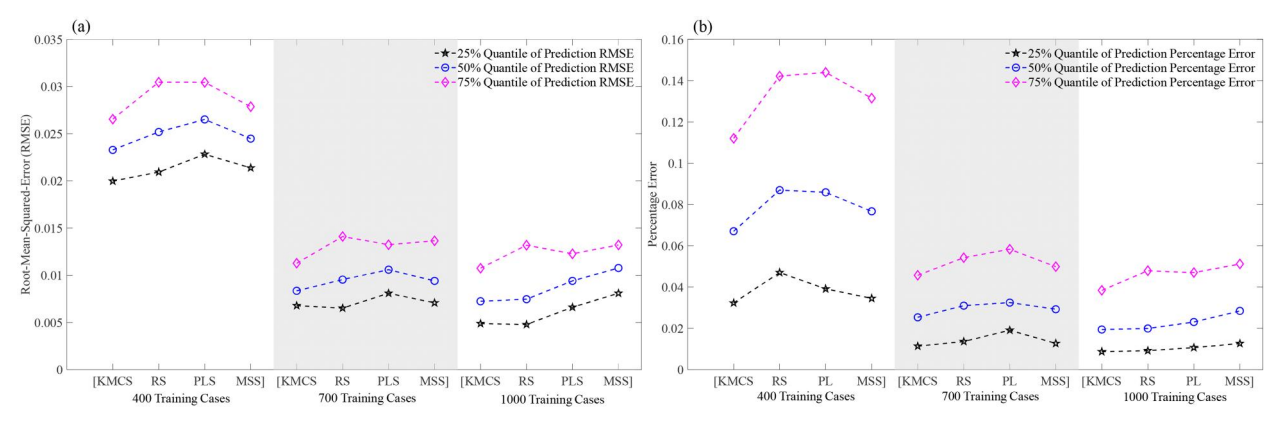


Figure 23. Comparison of the efficiency of the one-tower two-span surrogate model with different training sizes: (a) root mean square error; (b) maximum top displacement.

Table 5. The mean values of the RMSE at different time sections and the standard deviation for each sampling method trained one-tower two-span surrogate model.

	Mean Value		75% quantile value	
	Absolute value	Difference to KMCS (%)	Absolute value	Difference to KMCS (%)
KMCS	0.0084	0.0000	0.0113	0.0000
RS	0.0095	14.3103	0.0141	25.1225
PLS	0.0106	26.8473	0.0132	17.4684
MSS	0.0094	12.6699	0.0137	21.1588

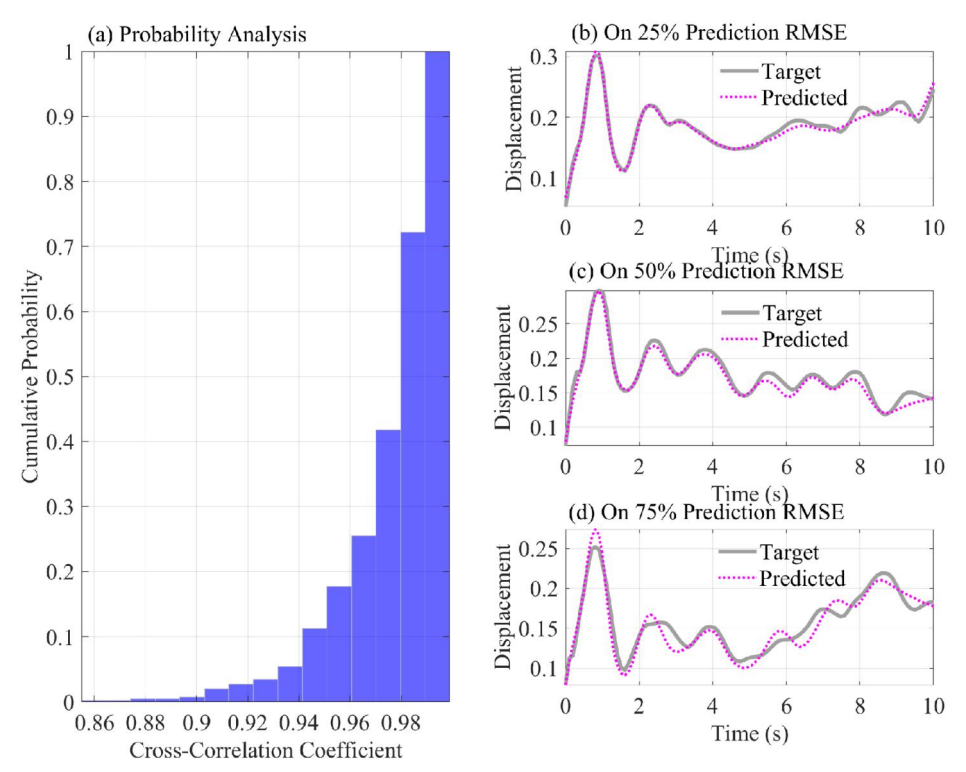


Figure 24. KMCS method trained one-tower two-span surrogate model prediction RMSE cumulative probability and the predicted time-history for accuracy testing.

changes to wind profile characteristics. The one-tower twospan surrogate models are trained by using wind profiles obtained on 26th of August at 04:30, while wind profiles from 26th of August at 08:30 are used to assess robustness. Figure 26 illustrates the RMSE of predicted displacement time histories for all sampling methods in the trained

surrogate models. Evidently from Figure 26, the KMCS method is the most effective approach for selecting representative wind profiles. Table 6 provides a summary of the comparison of RMSE for predicted displacement time histories across different sampling methods at the two timestamps. Notably, the mean and 75th percentile RMSE values

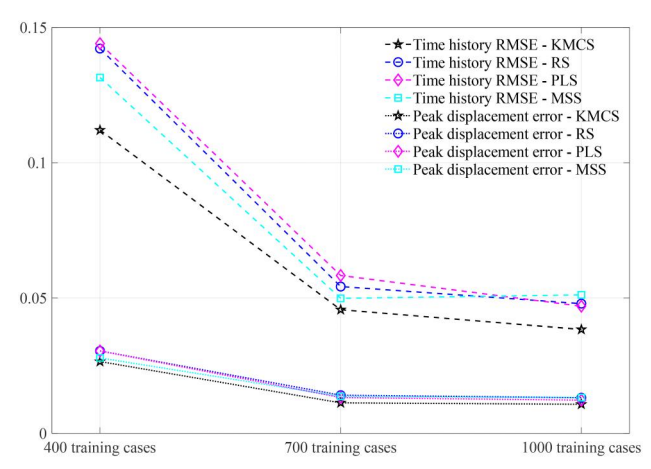


Figure 25. Comparison of the different sampling methods trained one-tower two-span surrogate model trained by 400, 700, and 1000 cases convergence rate for time history and peak displacement prediction.

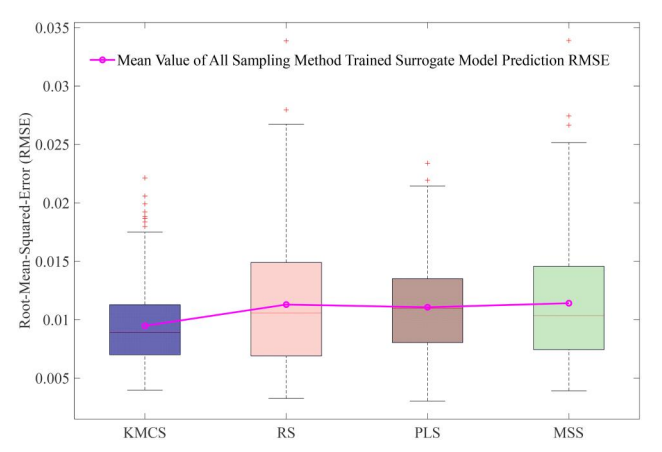


Figure 26. Robustness of the four sampling methods trained one-tower twospan surrogate model prediction RMSE on 26th of August at 08:30.

Table 6. Developed surrogate model robustness RMSE assessment on 26th of August at 08:30.

	Mean value		75% quar	75% quantile value	
	26th of	26th of	26th of	26th of	
	August	August	August	August	
	at 04:30	at 08:30	at 04:30	at 08:30	
KMCS	0.0089	0.0084	0.0113	0.0113	
RS	0.0106	0.0095	0.0149	0.0141	
PLS	0.0110	0.0106	0.0135	0.0132	
MSS	0.0104	0.0094	0.0146	0.0137	

for the evaluated timestamps are consistent across all sampling methods, indicating the robustness of the trained onetower two-span surrogate model.

6. Conclusions

In this paper, surrogate models of transmission tower-line systems are trained to predict the regional power infrastructure response in high-resolution wind fields during the evolution of Hurricane Harvey. The surrogate model predicts the dynamic response of a coupled nonlinear transmission tower-line system during wind loadings. Owing to the complexities in the wind loading characteristics introduced by both the auto- and cross-spectrum in the time history and the realistic profiles extracted from the wind fields. effective in-event surrogate model training algorithms are investigated.

Two transmission tower-line structure models with different levels of structural complexity have been utilised to verify the proposed surrogate model. The accuracy and robustness of these two models have been validated first. Then, to make the LSTM surrogate model applicable to all in-event reference wind speeds of the wind profiles, a single LSTM model is constructed. From the discussions, the following conclusions can be derived:

- The in-event surrogate training method decouples the extrinsic wind profiles from the intrinsic stochastic wind turbulence in the complex wind loading and investigates different sampling methods to select the training profiles effectively.
- The proposed surrogate training method is adaptive to structures with different levels of complexity. With different levels of structural complexity, the LSTM surrogate model hyper-parameters need to be adjusted to attain superior prediction accuracy.
- The number of training size is proportional to the number of LSTM units. Specifically, the two-tower one-span model utilised 400 training data samples alongside 96 LSTM units, while the one-tower two-span model employed a larger dataset comprising 1000 training data samples and 152 LSTM units. The observed relationship serves as a valuable guideline on how to appropriately configure the training dataset size and LSTM unit count for applying the proposed surrogate model training methodology diverse transmission tower-line structures.
- Among the four proposed data- and physics-based sampling methods, the k-medoids clustering sampling (KMSC) method outperforms other sampling methods in trained surrogate models, which leads to the benefits of using the in-event surrogate training method. Moreover, the physics-based power law sampling (PLS) is independent of the hurricane wind field, which leads to the potential to develop offline surrogate models for future hurricane events.
- The accuracy of the surrogate model is primarily overridden by the effectiveness of the surrogate model in capturing the transmission tower-line dynamic response given stochastic wind loading for small training dataset cases. With enough training cases, the effective selection and coverage of the wind profiles contribute to the accuracy of the surrogate models.
- With large training cases covering the entire in-event reference wind speed, the LSTM surrogate model can generalise the prediction of displacement time-history with acceptable accuracy. Hence, it is acceptable to extend the training and applying of the LSTM surrogate models to different transmission tower-line structures for regional scale transmission tower-line structure performance assessment.

Acknowledgements

This material is based upon the work supported by the National Science Foundation under award numbers 2004658 and 2121875. Any opinions, findings, conclusions, or recommendations expressed in this material are those of the author(s) and do not necessarily reflect the views of the National Science Foundation.

Disclosure statement

No potential conflict of interest was reported by the author(s).

References

- ASCE7-22. (2021). Minimum design loads and associated criteria for buildings and other structures. Reston, VA: American Society of Civil Engineers.
- Bi, W., Tian, L., Li, C., Ma, Z., & Pan, H. (2023). Wind-induced failure analysis of a transmission tower-line system with long-term measured data and orientation effect. *Reliability Engineering & System Safety*, 229, 108875. doi:10.1016/j.ress.2022.108875
- Chopra, A. K. (2012). Dynamics of structures: Theory and applications to earthquake engineering. Pearson Prentice Hall.
- Constantinescu, E. M., Zavala, V. M., Rocklin, M., Lee, S. M., & Anitescu, M. (2011). A computational framework for uncertainty quantification and stochastic optimization in unit commitment with wind power generation. *IEEE Transactions on Power Systems*, 26(1), 431–441. doi:10.1109/TPWRS.2010.2048133
- Davenport, A. G. (1961). The spectrum of horizontal gustiness near the ground in high winds. Quarterly Journal of the Royal Meteorological Society, 87(372), 194–211. doi:10.1002/qj.49708737208
- Dikshit, S., & Alipour, A. (2023). A moment-matching method for fragility analysis of transmission towers under straight line winds. Reliability Engineering & System Safety, 236, 109241. doi:10.1016/j. ress.2023.109241
- Fei, Q., Zhou, H., Han, X., & Wang, J. (2012). Structural health monitoring oriented stability and dynamic analysis of a long-span transmission tower-line system. *Engineering Failure Analysis*, 20, 80–87. doi:10.1016/j.engfailanal.2011.11.001
- Fu, X., Li, H.-N., Tian, L., Wang, J., & Cheng, H. (2019). Fragility analysis of transmission line subjected to wind loading. *Journal of Performance of Constructed Facilities*, 33(4), 04019044. doi:10.1061/(ASCE)CF.1943-5509.0001311
- Goodfellow, I. (2016). *Deep learning*. Cambridge, Massachusetts: The MIT Press.
- Hochreiter, S., & Schmidhuber, J. (1997). Long short-term memory. Neural Computation, 9(8), 1735–1780. doi:10.1162/neco.1997.9.8.1735
- Im, S., Lee, J., & Cho, M. (2021). Surrogate modeling of elasto-plastic problems via long short-term memory neural networks and proper orthogonal decomposition. Computer Methods in Applied Mechanics and Engineering, 385, 114030. doi:10.1016/j.cma.2021.114030
- Jeddi, A. B., Shafieezadeh, A., Hur, J., Ha, J.-G., Hahm, D., & Kim, M.-K. (2022). Multi-hazard typhoon and earthquake collapse fragility models for transmission towers: An active learning reliability approach using gradient boosting classifiers. *Earthquake Engineering & Structural Dynamics*, 51(15), 3552–3573. doi:10.1002/eqe.3735
- Kaufman, L. (1990). Finding groups in data: An introduction to cluster analysis. New York: Wiley.
- Kroetz, H. M., Tessari, R. K., & Beck, A. T. (2017). Performance of global metamodeling techniques in solution of structural reliability problems. *Advances in Engineering Software*, 114, 394–404. doi:10. 1016/j.advengsoft.2017.08.001
- Kwon, D. K., & Kareem, A. (2009). Gust-front factor: New framework for wind load effects on structures. *Journal of Structural Engineering*, 135(6), 717–732. doi:10.1061/(Asce)0733-9445(2009)135:6(717)
- Li, B., Chuang, W.-C., & Spence Seymour, M. J. (2021). Response estimation of multi-degree-of-freedom nonlinear stochastic structural

- systems through metamodeling. Journal of Engineering Mechanics, 147(11), 04021082. doi:10.1061/(ASCE)EM.1943-7889.0001963
- Li, B., & Spence Seymour, M. J. (2022). Metamodeling through deep learning of high-dimensional dynamic nonlinear systems driven by general stochastic excitation. *Journal of Structural Engineering*, 148(11), 04022186. doi:10.1061/(ASCE)ST.1943-541X.0003499
- Li, Q. S., Zhi, L., & Hu, F. (2010). Boundary layer wind structure from observations on a 325m tower. *Journal of Wind Engineering and Industrial Aerodynamics*, 98(12), 818–832. doi:10.1016/j.jweia.2010. 08.001
- Liao, Y. C., Lin, R., Zhang, R. Y., & Wu, G. (2023). Attention-based LSTM (AttLSTM) neural network for Seismic Response Modeling of Bridges. *Computers & Structures*, 275, 106915. doi:10.1016/j.compstruc.2022.106915
- Likas, A., Vlassis, N., & Verbeek, J. J. (2003). The global k-means clustering algorithm. *Pattern Recognition*, 36(2), 451–461. <Go to ISI>://WOS:000179225600015 doi:10.1016/S0031-3203(02)00060-2
- Ma, L. Y., Christou, V., & Bocchini, P. (2022). Framework for probabilistic simulation of power transmission network performance under hurricanes. *Reliability Engineering & System Safety*, 217, 108072. doi:10.1016/j.ress.2021.108072
- Ma, L. Y., Khazaali, M., & Bocchini, P. (2021). Component-based fragility analysis of transmission towers subjected to hurricane wind load. *Engineering Structures*, 242, 112586. doi:10.1016/j.engstruct. 2021.112586
- Mangalathu, S., Heo, G., & Jeon, J. S. (2018). Artificial neural network based multi-dimensional fragility development of skewed concrete bridge classes. *Engineering Structures*, *162*, 166–176. doi:10.1016/j. engstruct.2018.01.053
- Mazzoni, S., McKenna, F., Scott, M. H., & Fenves, G. L. (2006). OpenSees command language manual. *Pacific Earthquake Engineering Research (PEER) Center*, 264(1), 137–158.
- Mohammadi Darestani, Y., Shafieezadeh, A., & Cha, K. (2020). Effect of modelling complexities on extreme wind hazard performance of steel lattice transmission towers. *Structure and Infrastructure Engineering*, 16(6), 898–915. doi:10.1080/15732479.2019.1673783
- Natarajan, K., & Santhakumar, A. R. (1995). Reliability-based optimization of transmission-line towers. *Computers & Structures*, 55(3), 387–403. doi:10.1016/0045-7949(95)98866-O
- Oh, B. K., Glisic, B., Kim, Y., & Park, H. S. (2019). Convolutional neural network-based wind-induced response estimation model for tall buildings. Computer-Aided Civil and Infrastructure Engineering, 34(10), 843–858. doi:10.1111/mice.12476
- Oh, B. K., Glisic, B., Park, S. W., & Park, H. S. (2020). Neural network-based seismic response prediction model for building structures using artificial earthquakes. *Journal of Sound and Vibration*, 468, 115109. doi:10.1016/j.jsv.2019.115109
- Panteli, M., Pickering, C., Wilkinson, S., Dawson, R., & Mancarella, P. (2017). Power system resilience to extreme weather: Fragility modeling, probabilistic impact assessment, and adaptation measures. *IEEE Transactions on Power Systems*, 32(5), 3747–3757. doi:10.1109/TPWRS.2016.2641463
- Park, H. S., & Jun, C. H. (2009). A simple and fast algorithm for K-medoids clustering. Expert Systems with Applications, 36(2), 3336–3341. doi:10.1016/j.eswa.2008.01.039
- Shin, J., Scott, D. W., Stewart, L. K., & Jeon, J. S. (2020). Multi-hazard assessment and mitigation for seismically-deficient RC building frames using artificial neural network models. *Engineering Structures*, 207, 110204. doi:10.1016/j.engstruct.2020.110204
- Shinozuka, M., & Deodatis, G. (1991). Simulation of Stochastic Processes by Spectral Representation. Applied Mechanics Reviews, 44(4), 191–204. doi:10.1115/1.3119501
- Skamarock, C., Klemp, B., Dudhia, J., Gill, O., Liu, Z., Berner, J., ... Huang, X. (2019). (Eds.) A description of the advanced research WRF model Version 4. National Center for Atmospheric Research. doi:10.5065/1dfh-6p97
- Snaiki, R., & Wu, T. (2018). A semi-empirical model for mean wind velocity profile of landfalling hurricane boundary layers. *Journal of Wind Engineering and Industrial Aerodynamics*, 180, 249–261. doi: 10.1016/j.jweia.2018.08.004



- Tian, L., Zhang, X., & Fu, X. (2020). Fragility analysis of a long-span transmission tower-line system under wind loads. Advances in Structural Engineering, 23(10), 2110-2120. doi:10.1177/1369433220 903983
- TIGGE. The TIGGE dataset https://confluence.ecmwf.int/display/ TIGGE/Description.
- Torky, A. A., & Ohno, S. (2021). Deep learning techniques for predicting nonlinear multi-component seismic responses of structural buildings. Computers & Structures, 252, 106570. doi:10.1016/j.compstruc.2021.106570
- Tzortzis, G. F., & Likas, A. C. (2009). The Global Kernel k-Means Algorithm for Clustering in Feature Space. IEEE Transactions on Neural Networks, 20(7), 1181–1194. doi:10.1109/Tnn.2009.2019722
- Wang, J., Li, H. N., Fu, X., Dong, Z. Q., & Sun, Z. G. (2022). Wind fragility assessment and sensitivity analysis for a transmission tower-line system. Journal of Wind Engineering and Industrial Aerodynamics, 231, 105233. doi:10.1016/j.jweia.2022.105233
- Wang, J., Li, H. N., Fu, X., & Li, Q. (2021). Geometric imperfections and ultimate capacity analysis of a steel lattice transmission tower. Journal of Constructional Steel Research, 183, 106734. doi:10.1016/j. jcsr.2021.106734
- Wang, Z. Y., Pedroni, N., Zentner, I., & Zio, E. (2018). Seismic fragility analysis with artificial neural networks: Application to nuclear power plant equipment. Engineering Structures, 162, 213-225. doi: 10.1016/j.engstruct.2018.02.024
- WRF. Weather research and forecasting model. https://www.mmm.ucar. edu/weather-research-and-forecasting-model.
- Xie, Q., Cai, Y., & Xue, S. (2017). Wind-induced vibration of UHV transmission tower line system: Wind tunnel test on aero-elastic model. Journal of Wind Engineering and Industrial Aerodynamics, 171, 219-229. doi:10.1016/j.jweia.2017.10.011
- Xu, Y., Lu, X., Cetiner, B., & Taciroglu, E. (2021). Real-time regional seismic damage assessment framework based on long short-term

- memory neural network. Computer-Aided Civil and Infrastructure Engineering, 36(4), 504-521. doi:10.1111/mice.12628
- Xue, J., Mohammadi, F., Li, X., Sahraei-Ardakani, M., Ou, G., & Pu, Z. (2020). Impact of transmission tower-line interaction to the bulk power system during hurricane. Reliability Engineering & System Safety, 203, 107079. doi:10.1016/j.ress.2020.107079
- Xue, J., & Ou, G. (2021). Predicting wind-induced structural response with LSTM in transmission tower-line system. Smart Structures and Systems, 28(3), 391-405. doi:10.12989/SSS.2021.28.3.391
- Xue, J., Xiang, Z., & Ou, G. (2021). Predicting single freestanding transmission tower time history response during complex wind input through a convolutional neural network based surrogate model. Engineering Structures, 233, 111859. doi:10.1016/j.engstruct. 2021.111859
- Yates, F., & Thornton, H. G. (1948). Systematic sampling. Philosophical Transactions of the Royal Society of London. Series A, Mathematical and Physical Sciences, 241(834), 345-377. doi:10.1098/rsta.1948.0023
- Zhang, C., Song, C. L., & Shafieezadeh, A. (2022). Adaptive reliability analysis for multi-fidelity models using a collective learning strategy. Structural Safety, 94, 102141. doi:10.1016/j.strusafe.2021.102141
- Zhang, R., Chen, Z., Chen, S., Zheng, J., Büyüköztürk, O., & Sun, H. (2019). Deep long short-term memory networks for nonlinear structural seismic response prediction. Computers & Structures, 220, 55-68. doi:10.1016/j.compstruc.2019.05.006
- Zhang, R., Liu, Y., & Sun, H. (2020). Physics-informed multi-LSTM networks for metamodeling of nonlinear structures. Computer Methods in Applied Mechanics and Engineering, 369, 113226. doi:10. 1016/j.cma.2020.113226
- Zhu, X., & Ou, G. (2021). Investigation and development of a threedimensional transmission tower-line system model using nonlinear truss and elastic catenary elements for wind loading dynamic simulation. Shock and Vibration, 2021, 1-29. doi:10.1155/2021/1959683